

KOI-256's Magnetic Activity under the Influence of the White Dwarf

Ezgi YOLDAŞ^{1,2}, Hasan Ali DAL¹

¹ Department of Astronomy and Space Sciences, University of Ege, Bornova, 35100 İzmir, Turkey

² Corresponding Author, Email: ezgiyoldas@gmail.com

Abstract: We present the findings about chromospheric activity nature of KOI-256 obtained from the Kepler Mission data. Firstly, it was found that there are some sinusoidal variations out-of-eclipses due to cool spot activity. The sinusoidal variations modelled by the SPOTMODEL program indicate that the active component has two different active regions. Their longitudinal variation revealed that one of them has a migration period of 3.95 years, while the other has a migration period of 8.37 years. Secondly, 225 flares were detected from the short cadence data in total. The parameters, such as increase (T_r) and decay (T_d) times, total flare time (T_i), equivalent durations (P), were calculated for each flare. The distribution of equivalent durations versus total flare times in logarithmic scale is modelled to find flare activity level. The *Plateau* value known as the saturation level of the active component was calculated to be 2.3121 ± 0.0964 s, and the *Half-life* value, which is required flare total time to reach the saturation, was computed to be 2233.6 s. In addition, the frequency of N_1 , which is the number of flares per an hour in the system, was found to be 0.05087 h^{-1} , while the flare frequency N_2 that the flare-equivalent duration emitting per an hour was found to be 0.00051. Contrary to the spot activity, it has been found that the flares are in tends to appear at specific phases due to the white dwarf component.

Keywords: techniques: photometric - methods: data analysis - methods: statistical - binaries: eclipsing - stars: low-mass - stars: flare - stars: individual (KOI-256).

1 Introduction

65% of the stars in our galaxy are red dwarf stars, and 75% of them show flare activity (Rodonó 1986). The vast majority of the red dwarfs found in the open star clusters and association show flare activity (Mirzoyan 1990; Pigatto 1990), while the number of UV Ceti stars in the clusters decrease from a young cluster to the older one (Skumanich 1972; Marcy & Chen 1992; Pettersen 1991; Stauffer 1991). The flare activity results in mass loss, which plays an important role in stellar evolution.

Although various studies have been carried out since the first flare was observed by R. C. Carrington and R. Hodgson on September 1, 1859 (Carrington 1859; Hodgson 1859), it is not fully understood what the flare and its process are. However, the flare activity of the dMe stars is modelled on the basis of the Solar Flare Event (Gershberg 2005; Benz & Güdel 2010). The studies, which have been continuing to understand the flare events of dMe stars have revealed that there are some differences between the flare energy levels of stars (Gershberg & Shakhovskaya 1983).

The level of highest energy releasing on the Sun are about 10^{30} - 10^{31} erg in the flare events (Gershberg 2005; Benz 2008). It seems that this level is about 10^{31} erg (Haisch et al. 1991), if RS CVn stars, the chromospheric active binaries, are considered. The observations lasting over decades show that the energy levels of flares occurring on dMe stars could have increased from 10^{28} erg to 10^{34} erg (Gershberg 2005). Considering the stars in the Pleiades cluster and Orion asso-

ciation, it is seen that these values have reached 10^{36} erg (Gershberg & Shakhovskaya 1983). There are significant differences between the energy level of flare stars from different spectral types. For example, it is well known that there are serious differences between the mass loss rates and the flare energy level, if the Sun is compared to a dMe star. Nevertheless, the flare events occurring on the dMe stars are tried to be explained with the Solar Flare processes. As a result, it is clear that the flares in the different stars should be well studied and the similarities and differences between them should be analyzed. Gershberg (2005) and Hudson & Khan (1997) have suggested that magnetic reconnection processes are the source of energy for flare events. In order to determine the important points in the flare process, it is necessary that the cause of the differences in the flare frequency and also the flare energy spectra should be determined.

Besides Gershberg & Shakhovskaya (1983), there are several studies about the flare energies in the literature such as Gershberg et al. (1972); Lacy et al. (1976); Walker (1981); Pettersen et al. (1984); Mavridis & Avgolouropoulos (1986). However, according to Dal & Evren (2010, 2011), the results obtained in these studies are unsatisfactory for comparing the stars from different spectral types. For example Gershberg et al. (1972) derived the flare energy spectra for several dMe stars, such as AD Leo, EV Lac, UV Cet and YZ CMi, while Gershberg & Shakhovskaya (1983) derived the flare energy spectra for lots of stars from the galactic field to compare with the flare energy spectra of some stars from Pleiades and Orion association. They showed

that these stars are located in different points in the distribution of energy. They correctly indicated that this distribution is caused due to different ages of the stars. On the other hand, Dal & Evren (2010, 2011) indicated that there is one more reason to cause this distribution. The second reason is including the luminosity parameter in calculations, of flare energies, which leads to incorrect results, as this caused the stratifying in the flare energy spectra. Indeed, the studies of Dal & Evren (2010, 2011) show that the flare equivalent durations in the logarithmic scale vary within a certain rule versus the flare total time, and it depends on the spectral type of the stars, on which the flares occur, when the relations between the flare parameters are examined. On the other hand, two different flare frequencies were defined by Ishida et al. (1991) for the flare activity. The frequency of N_1 indicates the number of flares per an hour, while the frequency of N_2 describes the flare-equivalent duration emitting per an hour. Leto et al. (1997) clearly show that the frequency of EV Lac's flares vary over time.

On the other hand, for the first time in the literature, Kron (1952) discovered that UV Ceti-type stars also exhibited spot activity known as BY Dra Syndrome. Kron (1952) observed sinusoidal variations out-of-eclipses in the light curves of the YY Gem, which is a binary system, and Kunkel (1975) called this phenomenon BY Dra Syndrome and explained as a fact that these variations were caused by heterogeneous temperature distribution on the surface of the star. In the case of the Sun, Berdyugina & Järvinen (2005) found two stable active longitudes separated by 180 degrees from each other, and they indicated that these longitudes are exhibiting semi-rigid behavior. However, according to some authors, these longitudes are not the persistent active structures, which show variation in the time (Lopez 1961; Stanek 1972; Bogart 1982). The difference between the regular activity oscillations shown by these longitudes, called the Flip-Flop, is very important for the north-south asymmetry exhibited by the star's magnetic topology. It is very important to calculate the angular velocities of these longitudes because these calculations light on the differential rotational velocities in the latitudes of the spots and spots groups.

In the case of binary or single stars, determining the parameters of stellar spot activity, such as spot latitude, radius and longitude, is a controversial phenomenon. In the literature, there are several methods to find out these parameters (Ribárik 2002; Ribárik et al. 2003; Walkowicz et al. 2013a; Jeffers & Keller 2009). For example, the SPOTMODEL program (Ribárik 2002; Ribárik et al. 2003) required two band observation and the inclination of the rotation axis to be able to model the distribution of the spots on the stellar surface. However, it must be noted that the system's maximum brightness level ever observed has also a very important role to determine the spot radius depending on spot latitude. According to Walkowicz et al. (2013a); Jeffers & Keller (2009), this method does not work for the observations such as the data acquired in the Kepler Mission. Because the Kepler observations provide us monochromatic data, which have been detrended

while combining different observation parts.

In this study, we examine the flare and spot activity exhibiting by KOI-256, and examine the parameters derived from the One Phase Exponential Association (hereafter OPEA) model, and also the spot migration considering the sinusoidal variation out-of-the flare. It is seen from the literature that KOI-256 is a system, which the primary component is a white dwarf, the secondary component is a main sequence star from the spectral type of M3. In addition, there are some clues about third body, which could be a planet. Borucki et al. (2011) indicated that KOI-256 is a planet candidate system. There are lots of studies such as Ritter & Kolb (2003); Borucki et al. (2011); Slawson et al. (2011); Walkowicz & Basri (2013b); Muirhead et al. (2013, 2014); Zacharias et al. (2004) in the literature. Several physical parameters of KOI-256 were computed in these studies, using some colour calibrations explained by these authors. As it can be seen from these parameters listed in Table 1, KOI-256 is very interesting system. Although one of the components is a with dwarf, Walkowicz & Basri (2013b) indicated that the system's age is 0.01 Gyr. However, using the Equation 2.3 given by Gänsicke (1997) with the stellar parameters taken from Muirhead et al. (2013), we estimated the age of the system as ~ 2 Gyr, considering the cooling of the white dwarf component. Indeed, Muirhead et al. (2013) later revealed that the system is a post-common envelope binary. In the paper, the stellar spot activity analyses are described in Section 2.1, while the flare models are described in Section 2.2. The orbital period variation analysis is explained in Section 2.3. The results obtained from the analyses are summarised and discussed in Section 3.

2 Data and Analyses

The Kepler Mission project, which was launched to explore the exoplanets, has observed more than 150.000 sources (Borucki et al. 2010; Koch et al. 2010; Caldwell et al. 2010). These observations are one of the highest sensitivity photometric observations ever achieved (Jenkins et al. 2010a,b). With this highest sensitivity of observation, a large number of new eclipsing binaries and lots of new variable stars have been discovered besides the exoplanets (Slawson et al. 2011; Matijevič et al. 2012). Some of these variable stars are single, and some of them are binary stars, which exhibit both the stellar spot activity and flare activity (Balaji et al. 2015). In this study, observational data of KOI-256, which is one of these binary systems, was taken from Kepler Data Base (Slawson et al. 2011; Matijevič et al. 2012). KOI-256's short cadence data obtained in the Kepler Mission covered the time range from BJD 24 55372.460219 to BJD 24 55552.55836 and from BJD 24 56419.80351 to BJD 24 56424.01160, while the long cadence data of the system covered time ranges BJD 24 54964.51238-55206.21898, BJD 24 55276.51124-55552.54849, BJD 24 55641.51645-55931.30552, BJD 24 56015.77828-56304.13695, BJD 24 56392.24699-56424.00173. All the available data presented in both Long and Short Cadence formats are shown in Figure 1. The short

cadence data were used in the analyses of the flares, while the long cadence data were used for the analyses of sinusoidal variation. The detrended data was used among the public data provided in the Kepler Data Base. The data sets were created in appropriate formats, which were edited in the analysis processes for the flare activity, the stellar spot activity and the orbital period variation ($O - C$).

The whole of KOI-256's analysed data taken from the Kepler Database is shown in the upper and middle panels of Figure 1. The light curve is plotted versus the Barycentric Julian Date in the upper panel, while it is plotted versus phase in the middle panel of the figure. In the lower panel, the light curve is plotted versus phase, expanding the y-axis to be easily seen the sinusoidal variations out-of-the dominant flare activity.

2.1 Stellar Spot Activity

Examining the out-of-eclipses light variations, it is seen that the system exhibits also sinusoidal variations. Considering the surface temperatures of the components of the system, it is understood that the variations are caused by the rotational modulation of the cool stellar spots. It is seen that both minima times and amplitudes of the light curves are varying once in a few cycles, when the consecutive cycles depend on the orbital period are examined in the light curves, in which both the flares and eclipses are removed. This situation indicates that the active regions on the components of the system evolved rapidly. Because of this, it is not possible to model the entire light curve in a single analysis, so the data of sinusoidal variation are separated into several sets. When dividing into data sets, consecutive cycles in which some characters of the light curve such as a light curve asymmetry, a spot minima phase, and the minima and maxima level were the same were collected in a single set. In this format, 138 sub-sets are obtained, thus, each sub-set is modelled separately.

To be able to model the sinusoidal variations, the pre-whitened light curves were obtained. In this step, we firstly removed data parts, in which all instant light increase due to the flares are seen, from whole data. In addition, the data parts, in which the primary minima are seen due to eclipses, were also removed from whole data.

The pre-whitened light curves are modelled with the SPOTMODEL program (Ribárik 2002; Ribárik et al. 2003) to find out the spot distribution parameters, such as the spot radius, latitude and especially longitudinal distribution, on the stars. To model the spots, the SPOTMODEL program requires two band observations or a temperature factor ($kw = [T_{spot}/T_{stellarsurface}]^2$) and to find out the flare behaviour of the system, we tried to determine the flares occurring on the active component. For the reason, using the synthetic light curves, all the other variations apart from the flares were removed from the entire light curve. Since the system is an eclipsing binary, all minima light variations between the phases of 0.04 around the minima points, where two components are external tangent to each other, were removed from the entire light curve. However, the separated observations due to the technical reasons were also removed from the data.

by Muirhead et al. (2013). Then, taking the different values from $kw = 0.60$ to $kw = 0.90$ for the spot temperature factor in agreement with the values found by these studies for analogue systems, the first few sets were tried to be modelled. As a result, it was seen that the best solution can be obtained by taking the spot temperature factor of $kw = 0.65$ for both spots. For this reason, the spot temperature factors were taken as $kw = 0.65$ for both spots in the all sets. Taking the spot temperature factor as constant value in the models for each set, the longitudinal, latitudinal distributions and radius variations of the spot area on the active component were determined.

In the analysis, the parameters such as the longitudes (l), latitudes (b), and radii of the spots (g) parameters were taken as free parameters. The parameters obtained from the models for each set are listed in Table 2, while six examples for the derived models are shown in Figure 2. In the left panel of the figure, the observations and models are plotted versus Heliocentric Julian Day as a time, while they were plotted versus phase computed using by orbital period. As seen from the figure, the synthetic models absolutely fit the observations. The variations of latitude (b) and radius (g) for both spots are shown in Figures 3. In addition, the most important parameter of the models, longitude (l), is plotted versus time in Figure 4. The longitudinal variations were fitted by a linear function for both spots. Using these linear fits, the migration periods were computed. The migration period was found to be 3.95 year for first spotted area, and 8.37 year for second area.

To test whether the findings about longitudinal variations are close to the real nature of the stellar surface, it was tested by another method. Using the Fourier Transform, the minima times of sinusoidal variations, where the amplitude is larger, were computed. Then, the orbital phases called as θ_{min} were computed for these sinusoidal minima times. In figure 5, the variation of θ_{min} are plotted versus time. This variation was fitted by a linear function similar to the longitudinal variations. In the same process, the migration period was computed from the phase shift of the θ_{min} using this linear function. In a result, the period of the spotted area migration was found to be 9.126 year. As it is expected, this value is in agreement with one of the migration periods found from the longitudinal variations.

2.2 Flare Parameters and Models

In order to understand the nature of the flare activity and to find out the flare behaviour of the system, we tried to determine the flares occurring on the active component. For the reason, using the synthetic light curves, all the other variations apart from the flares were removed from the entire light curve. Since the system is an eclipsing binary, all minima light variations between the phases of 0.04 around the minima points, where two components are external tangent to each other, were removed from the entire light curve. However, the separated observations due to the technical reasons were also removed from the data.

In order to specify the flare parameters, such as start and end points of a flare and its energy, it should be defined the quiet level of the light curve. However, it was seen some sinusoidal variations due to the rotational modulation exhibited by one of the components in addition to the flares. For this reason, the synthetic light curves were derived for the light variations out-of-the flares using the Fourier transform given by Equation (1), and all the data were modelled with these synthetic light curves for the all phases.

$$L(\theta) = A_0 + \sum_{i=1}^N A_i \cos(i\theta) + \sum_{i=1}^N B_i \sin(i\theta) \quad (1)$$

here A_0 is the zero point, θ is the phase, while A_i and B_i are the amplitude parameters (Scargle 1982). The synthetic light curves derived by Equation (1) were assumed as the quiescent level for each flare. Two examples for the flares detected from the observations and their quiescent levels are shown in Figure 6. After modelling light variations out of both the eclipses and flares, the flare parameters are calculated, as it was previously described by Dal (2012) in detail.

The flare rise (T_r) and decay (T_d) times, the flare amplitudes and the equivalent durations (P) were calculated after the start and end points of a flare were determined. These flare parameters calculated for each flare detected from entire data sets are listed in Table 3. In this table, the times of flare maxima in the first column, the flare equivalent durations (s), the flare rise times (s), the flare decay times (s), the flare total times (s) and the flare amplitudes in the last column were listed, respectively.

225 flares in the total were detected from the available observational data of the system taken from the Kepler Database. The equivalent duration values for each flare are calculated by Equation (2) given by Gershberg et al. (1972).

$$P = \int [(I_{flare} - I_0)/I_0] dt \quad (2)$$

where P is the flare equivalent duration in seconds, I_{flare} is flux at the moment of a flare, and I_0 is the flux of the system in the quiescent level, which were modelled by the Fourier method for the parts out-of-eclipses. Considering the reason explained by Dal & Evren (2010, 2011), which is mentioned in Section 1, the flare energies were not used in this study. In order to derive the models, the equivalent duration parameter was used instead of the flare energy. Using the orbital period of the system, the phases for each flare was calculated, and the phase distribution of these 225 flares is shown in Figure 7. In the figure, it is plotted the flare total number computed for each phase range of 0.10.

When the relationship between some flare parameters is examined, it can be seen that the flare equivalent duration varies versus the flare total time within a certain rule. In fact, as it had been demonstrated by

Dal & Evren (2010, 2011), the regression calculations processed with the SPSS V17.0 (Green et al. 1999) and GraphPad Prism V5.02 (Dawson & Trapp 2004) programs in this study show that the One-Phase Exponential Association (hereafter OPEA) is the best function to model the distribution of the flare equivalent durations in the logarithmic scale versus the flare total time. The OPEA function is a special function that has a term "Plateau" and is represented by Equation (3) (Motulsky 2007; Spanier & Oldham 1987):

$$y = y_0 + (Plateau - y_0) \times (1 - e^{-k \times x}) \quad (3)$$

where the parameter y is equivalent duration in the logarithmic scale, x is the total time of a flare, and y_0 is the theoretical equivalent duration in the logarithmic scale for the minimum flare total time, as it had been previously defined by Dal & Evren (2010). In other words, the parameter y_0 defines the minimum equivalent duration that someone can obtain for a flare occurring on the active component. Therefore, y_0 value depends on the brightness of the observed target and on the sensitivity of the used optical system. The *Plateau* value defines the upper limit of the equivalent durations for the flares observed on a particular star. According to Dal & Evren (2011), this parameter is defined as the saturation level for the flare activity in the observed wavelength range for the observed target.

Using the least-squares method, the distribution of the equivalent duration versus the flare total time was modelled by the OPEA function for the flares. The obtained model is shown in Figure 8 with a 95% confidence interval. The computed parameters from the OPEA model are listed in Table 4. The span value listed in the table is the difference between *Plateau* and y_0 values. The *half-life* value is half of the first x value, which the flare equivalent durations in the logarithmic scale reach the maximum level defined as the *Plateau* value. In other words, it is half value of the first total time, where the highest flare energy is seen for the flare.

In the Kepler Mission database, KOI-256's short cadence data are available for the time range from BJD 24 55372.460219 to BJD 24 55552.55836 and from BJD 24 56419.80351 to BJD 24 56424.01160. In total, the KOI-256 has been observed in **short cadence format** during 184.30624 days (4423.34976 hours). From these data, 225 flares were obtained and their total equivalent durations were computed of 8169.834 seconds. In the literature, two different flare frequencies were defined by Gershberg et al. (1972). These frequencies are given by Equation (4, 5):

$$N_1 = \Sigma n_f / \Sigma T_t \quad (4)$$

$$N_2 = \Sigma P / \Sigma T_t \quad (5)$$

where Σn_f is the total number of the obtained flare, while ΣT_t defines the total observing time of the star. ΣP_u is the sum of the equivalent durations of all detected flares. According to these definitions, the N_1 frequency was found to be 0.05087 h^{-1} , while the N_2 frequency was found to be 0.00051 .

Gershberg et al. (1972) described the flare frequency distribution separately calculated for the different energy limits of the flares detected from a star, which defines the flare energy character for that star. However, using the flare equivalent duration instead of the flare energy parameter in this study, since the flare energy parameter depends on the quiet intensity level of the star in the observing band, the flare frequencies were calculated for different flare equivalent duration limits for the 225 flares. The obtained cumulative flare frequency distribution is shown in Figure 10.

2.3 Orbital Period Variation

The minima times were computed from the KOI-256s short cadence data from the first quarter to the Quarter 17, which were taken from the publicly available Kepler Database, without any corrections. The minima times were computed with a script depending on the method described by Kwee & van Woerden (1956). In this method, taking symmetrically increasing and decreasing parts of minima, the minima times were computed by fitting this parts with polynomial function. Before computing the minima times, the flares as the activity exhibited by the system were removed from the light curves. In the second step, $(O - C)I$ residuals were determined for the obtained minima times. However, some of them include very large errors. It is seen that the flare activity occurred during these minima, when the light curves were examined for these minima times with large errors. Thus, these minima times were removed from the $(O - C)$ data. As a result, 125 minima times were determined in the analyses. The obtained $(O - C)I$ residuals were adjusted by the linear correction given in Equation (6):

$$JD (Hel.) = 24\,54965.55513(4) + 1^d.3786503(1) \times E. \quad (6)$$

The computed minima times $(O - C)I$ and the $(O - C)II$ residuals obtained by applying a linear correction are listed in Table 5. In the table, the minima times, cycles, the minima type, $(O - C)I$ and $(O - C)II$ residuals are listed, respectively. An interesting variation is seen in the variation of obtained $(O - C)II$ residuals versus time in Figure 11.

Firstly, checking the minima types given in the third column of Table 5, it was practically examined whether there is a marker about the existence of secondary minimum, which is the subject of discussion in the literature. Secondly, it was examined whether there was any separation in the $(O - C)II$ residuals plotted in Figure 11. If there was any secondary minimum, it would be expected a separation between the primary and secondary minima time residuals due to stellar spot activity, as it was demonstrated by Tran et al.

(2013) and Balaji et al. (2015) for the first time. However, as it is seen from Figure 11, there is no decomposition in the minima time residuals as the primary and secondary minima.

3 Results and Discussion

The analysis of KOI-256s data taken from the Kepler Database (Slawson et al. 2011; Matijević et al. 2012) indicates that the system has high chromospheric activity. However, it is necessary to compare the activity level between similar stars in order to reach a more definite result about the activity nature. In the literature, KOI-256 is an eclipsing binary system, with a white dwarf as a primary component and a main sequence star from M3 spectral type as a secondary component (Muirhead et al. 2014). The temperatures of the components were determined as $T_1 = 7100 \text{ K}$ and $T_2 = 3450 \text{ K}$ in the analyses of the spectral data together with the photometrical data of the system (Muirhead et al. 2014).

The eclipsing binary system KOI-256 was observed in **the short cadence format** from HJD 24 54964.51238 to HJD 24 56424.011602 in total of 184.30624 days (4423.34976 hours). Within this study, 225 flares were determined and the parameters of each flare were calculated. Using the frequency descriptions defined by Gershberg et al. (1972), the flare frequencies for KOI-256 were calculated as $N_1 = 0.05087 \text{ h}^{-1}$ and $N_2 = 0.00051$, respectively. The flare frequencies of KOI-256 were compared with the flare frequencies found from the young main sequence dMe dwarfs, known as UV Ceti-type, exhibiting flare activity. The flare frequencies of KIC 9761199 were found to be $N_1 = 0.01351 \text{ h}^{-1}$ and $N_2 = 0.00006$ (Yoldaş & Dal 2016), while they were found to be $N_1 = 0.01735 \text{ h}^{-1}$ and $N_2 = 0.00001$ for KIC 9641031 (Yoldaş & Dal 2017). KOI-256, when compared to these two systems, seems to have the highest flare frequency values among similar systems. On the other hand, the N_2 frequencies were computed to be 0.088 for EQ Peg and 0.086 in the case of AD Leo, while the N_1 frequencies were determined as 1.331 h^{-1} for AD Leo, a UV Ceti type single star, and 1.056 h^{-1} for EV Lac (Dal & Evren 2011). Compared to these single stars of the UV Ceti type, the flare frequencies of KOI-256 are found to be quite low. However, it is known in the literature that the flare frequency of EV Lac varies with time (Leto et al. 1997). As it is seen in Figure 9, the monthly frequencies vary with time like EV Lac, when the flare frequencies are computed for each month in the case of KOI-256.

The *Plateau* value of the OPEA model depending on the flare equivalent duration distribution in the logarithmic scale versus the flare total time is found to be $2.3121 \pm 0.0964 \text{ s}$ over detected 225 flares. This value is 3.014 s for EV Lac ($B - V = 1^m.554$), 2.935 s for EQ Peg ($B - V = 1^m.574$) and 2.637 s for V1005 Ori ($B - V = 1^m.307$) (Dal & Evren 2011). The *Plateau* value was found to be $1.232 \pm 0.069 \text{ s}$ for KIC 9641031 ($B - V = 0^m.74$) (Yoldaş & Dal 2016) and $1.951 \pm 0.069 \text{ s}$ for KIC 9761199 ($B - V = 1^m.303$) (Yoldaş & Dal 2017). If it is considered that one of the components is a white

dwarf in the case of KOI-256, it is clear in this study that the chromospheric active component is the main sequence star from the spectral type of M3. The B-V color index for this component is given as ($1^m.42$) in the literature (Walkowicz & Basri 2013b). Therefore, the flares with high energy exhibited by KOI-256 are strong enough to be compared with the flares exhibited by the single UV Ceti type stars. Dal & Evren (2011). found that the *Plateau* value is constant for a star, but varies from one star to another depending on their $B - V$ color indexes. The authors have defined this value as the saturation level of flares on a star, which is maximum energy limit a flare can reach.

On the other hand, the *half-life* parameter of the OPEA model was found to be 2233.6 s for KOI-256. This value is almost 10 times higher than the value obtained on single flare stars. This value is 433.10 s for DO Cep ($B - V = 1^m.604$), 334.30 s for EQ Peg and 226.30 s for V1005 Ori (Dal & Evren 2011). In the same way, the *half-life* parameter is 2291.7 s for KIC 9641031, while it is 1014 s for KIC 9761199, which are binary systems including a dMe type component (Yoldaş & Dal 2016, 2017). As a result, when the flare total time for the stars such as EQ Peg, V1005 Ori and DO Cep reaches a few minutes, the their flare energies can easily reach the Plateau level. However, in the case of KOI-256, a flare event must last at least 37 minutes, about a few tens of minutes, in order to reach the maximum flare energy described as the Plateau level for this system. Similar durations are also observed in the case of both flare rise and total times. The maximum flare rise time (T_r) observed in the single UV Ceti type stars is about 2042 s for V1005 Ori, 1967 s for CR Dra (Dal & Evren 2011), while the longest flare rise time obtained in KOI-256 is 3942.749 s. The longest flare rise time obtained flares on KIC 9641031 is 5178.87 s (Yoldaş & Dal 2016), while it is 1118.099 s for KIC 9761199 (Yoldaş & Dal 2017). Similarly, the maximum flare total time for the flares obtained on the V1005 Ori is 5236 s, while it is 4955 s for CR Dra flares (Dal & Evren 2011). However, the longest flare obtained on KOI-256 lasts along 22185.361 s.

Considering the stellar spot activity together with the flare activity detected from KOI-256, it is obvious that the system exhibits a high level of chromospheric activity. Using very sensitive observations provided by Kepler Mission (Jenkins et al. 2010a,b), some variations with small amplitudes, which are impossible to observe with ground-based classic telescopes, can be easily detected. When the system light variations out-of-eclipses without any flares is carefully examined, it is seen that the shape of eliminated light curve can vary per two or three cycles at most. This variation is caused due to both rapid evolutions and migrations of the cool stellar spots on the surface of the M3 star. It needs about 4-5 days for the evolution of the stellar spots on the active component in the case of KOI-256, while it takes a few weeks for the cool spot groups on the solar surface (Gershberg 2005). In this study, the stellar spot distribution on the surface of the active component was modelled by the SPOTMODEL program (Ribárik 2002; Ribárik et al. 2003), though there are some deficiency in the method of this program. As

it was mentioned in Section 1, the method using in the SPOTMODEL program do consider neither the spot evolution nor spot migration on the surface during long time. However, separating the data into suitable sub-sets by considering the light curve shape change point, we solved out this problem. The whole data were separated into 138 sub-sets. The cycle shapes of sinusoidal light variation are different from one sub-set data to the next, while the shapes of the cycles are the same among themselves in each sub-set data. Thus, each sub-set data was individually modelled. On the other hand, maximum level of the obtained brightness is not suitable for modelling by the SPOTMODEL program due to detrended data. However, the spot longitude parameters is calculated in this study, because it is an important parameter to reveal the spot migration instead of the spot latitude or radius.

The result parameters of the modelling spot variation are plotted in Figures 2, 3 and 4. As it is seen from Figure 2, the models of 138 sub-sets indicate that two cool spots (or spotted areas) are enough to absolutely fit the observed light variation out-of-eclipses. Although both latitude and radius parameters of the spots do not externalize the realistic nature of the spots on the stellar surface as discussed earlier, their variations are also plotted in Figure 3 to note as an initial approach. The main goal of these models is longitudinal variation and it is shown in Figure 4. Observations of the cool spot groups on solar surface reveal the existence of two permanently active longitudes separated by 180 degree from each other. These active longitudes known as the Carrington Coordinates are constant structure according to some authors, while some authors indicate that the rotation speeds of these active longitudes are not constant, but slowly change (Lopez 1961; Stanek 1972; Bogart 1982). Similarly, in this study, it was found that there are two stellar cool spots on the active component of KOI-256, which show the migration behaviour with different speeds. Modelling the migration movements shown in Figure 4 by the linear fits, it is estimated that the migration of the first stellar spot is 3.95 years and the migration period of the second one is 8.37 years.

To test whether these results are real, it was tested by another method. Computing θ_{min} parameter, which is the phases of the observed sinusoidal variation out-of-eclipses, the migration behaviour of the dominant spotted area was tried to find out. Indeed, as it is seen from Figure 5, the θ_{min} values obtained for all cycles were plotted versus Heliocentric Julian Day, and then, its trend was fitted by a linear function. The migration period of dominant spotted area is found to be 9.13 year. In addition, the most impressive finding was came from the residual θ_{min} according to the linear fit. The residuals show the same trend with the residuals of the longitudinal variation obtained from the SPOTMODEL analyses. This situation absolutely reveals that the main goal of the SPOTMODEL analyses have been obtained, and it does figure out the migration of active regions close to its real nature.

However, as can be seen in Figure 4, some sinusoidal variations still remain, after a linear correction is applied to the migration movement. All of these

migration behaviours are an indicator of the strong differential rotation on stellar surface. However, a high-resolution spectroscopic observation is needed to confirm this case. In the literature, the system's age is given as 0.01 Gyr by Walkowicz & Basri (2013b). However, as it is described in Section 1, using the Equation 2.3 given by Gänsicke (1997) with the stellar parameters taken from Muirhead et al. (2013), the age of the system is estimated as ~ 2 Gyr in this study. Considering the law expressed by Skumanich (1972), this age is a bit old for rapid rotation, considering high level chromospheric activity. However, KOI-256 is a binary system. In this case, tidal effects can let the components to rotate rapidly, which lets the system has a significant influence on both the flare and spots activity behaviour.

Muirhead et al. (2014) listed the semi-major axis length of the system as $a = 4.51 R_{\odot}$, giving the radii of components as $R_1 = 0.54 R_{\odot}$ and $R_2 = 0.01 R_{\odot}$. This situation indicates that the components are very close to each other, which can cause rapid activity variations due to some tidal effects on each other. On the other hand, the most interesting result in term of stellar spot and flare activity exhibited by the system is that the stellar spot areas exhibit a rapid variation in location due to the migration movement as shown in Figure 5, while it is seen interestingly that the flares are in aim to occur frequently between the phases of 0.10 - 0.20 and also 0.60 - 0.70, when the averaged phases are calculated in each 0.10 phase range for 225 flares. In the case of both spot and flare activities, the phases were computed with using the orbital period of binary system with a white dwarf and a main sequence M3 components. This case is an unexpected situation, because the locations of flares are quite stable compared to the behaviour of the spot activity. Although flare activity is seen in all phases, it is observed that the flare activity most frequently occurs in these phase intervals. The location of the white dwarf is as close as $4.51 R_{\odot}$ to the active component, which indicates that the components are interacting magnetically. A possible explanation is that the quickly evolving stellar spot areas under both the differential rotation and tidal effects exhibit rapid migration movements, while the flares are frequently occurring in some definite longitudes on the active component surface due to the magnetic interaction of the white dwarf and active components. This situation leads KOI-256 to take an important position among its analogues for especially the future spectral studies.

125 minima times were determined from the all available data. It is seen that the light curve has only the primary minimum, when entire the light curves are examined. According to Tran et al. (2013) and Balaji et al. (2015), the $(O - C)II$ residuals of the primary and secondary minima show some sinusoidal variation versus time, but in the opposed phase, if one of the components in an eclipsing binary system is a magnetically active star. However, the $(O - C)II$ residuals obtained from the minima detected from the light curves of KOI-256 do not exhibit any separation. This situation also confirms that all the minima detected from the light curves are primary ones.

As it is seen from Figure 11, considering all 125 minima times, there is not any clear variation in the $(O - C)II$ residuals distribution versus time obtained by improving linear correction. As shown in Figure 11, the $(O - C)II$ residuals scatter in a range of about 50-60 sec. Whereas according to Szabó et al. (2013) in the literature, KOI-256 shows an $(O - C)II$ variation with an amplitude of 0.4464 minute and a period of 41.755397 day. However, the results obtained in this study do not confirm the variation found by Szabó et al. (2013). **The problem, which cause the different results can be due to the method used to compute the minima times or due to the different data formats used in these studies. In this study, the minima times were computed from the short cadence data, while the minima times were calculated from the long cadence data by Szabó et al. (2013).** In addition, although the flares as the activity exhibited by the system were removed from the light curves before computing the minima times, the sinusoidal variation due to the stellar spot activity was not cleared from the data in order to test whether the primary and secondary minima were separated, as described by Tran et al. (2013) and Balaji et al. (2015). Although there is no any clue for the secondary minima, the situation can cause a scattering in a wide range for the $(O - C)II$ residuals variation obtained in this study.

Acknowledgments

We wish to thank the Turkish Scientific and Technical Research Council for supporting this work through grant No. 116F213. We also thank the referee for useful comments that have contributed to the improvement of the paper.

References

- Balaji, B., Croll, B., Levine, A. M., Rappaport, S., 2015, MNRAS, 448, 429
- Balona, L. A., 2015, MNRAS, 447, 2714 Balona, L.A., 2015, MNRAS, 447, 2714
- Benz, A. O., & Güdel, M. 2010, ARA&A, 48, 241
- Benz, A. O., 2008, Living Rev. Solar Phys., 5, 1
- Berdugina, S. V. & Järvinen, S. P., 2005, AN, 326, 283
- Bogart, R. S. 1982, Sol. Phys., 76, 155
- Borucki, W. J., Koch, D., Basri, G., et al., 2010, Sci, 327, 977
- Borucki, W.J., Koch, D.G., Basri, G., et al., 2011, ApJ, 736, 19
- Botsula, R. A., 1978, Perem. Zvezdy, 20, 588
- Caldwell, D. A., Kolodziejczak, J. J., & Van Cleve, J. E., 2010, ApJL, 713, L92

- Carrington, R. C., 1859, *MNRAS*, 20, 13
- Clausen, J. V., Helt, B. E., and Olsen, E. H., 2001, *A&A*, 374, 98
- Dal, H. A. & Evren, S., 2010, *AJ*, 140, 483
- Dal, H. A. & Evren, S., 2011, *AJ*, 141, 33
- Dal, H.A., 2012, *PASJ*, 64, 82
- Dawson, B., & Trapp, R. G., 2004, "Basic and Clinical Biostatistics" (New York: McGraw-Hill), 61
- Gershberg, R. E., & Shakhovskaya, N. I., 1983, *Astrophys. Space Sci.*, 95, 235
- Gershberg, R. E., 1972, *Astrophys. Space Sci.*, 19, 75
- Gershberg, R. E., 2005, "Solar-Type Activity in Main-Sequence Stars", Springer Berlin Heidelberg, New York, p.53, p.191, p.192, p.194, p.360
- Green, S. B., Salkind, N. J., & Akey, T. M., 1999, *Using SPSS for Windows: Analyzing and Understanding Data* (Upper Saddle River, NJ: Prentice Hall), 50
- Gänsicke, B. T., 1997, *PhDT*, 28.
- Haisch, B., Strong, K. T., Rodonó, M., 1991, *ARA&A*, 29, 275
- Hodgson, R., 1859, *MNRAS*, 20, 15
- Hudson, H. S., & Khan, J. I., 1997, in *ASP Conf. Ser.* 111, "Magnetic Reconnection in the Solar Atmosphere", ed. R. D. Bentley & J. T. Mariska (San Francisco, CA: ASP), 135
- Ishida, K., Ichimura, K., Shimizu, Y., & Mahasenaputra, 1991, *Ap&SS*, 182, 227
- Jeffers, S.V., Keller, C.U., 2009, *AIPC*, 1094, 664
- Jenkins, J. M., Caldwell, D. A., Chandrasekaran, H., Twicken, J. D., Bryson, S. T., Quintana, E., V., Clarke, B. D., Li, J., Allen, C., Tenenbaum, P., and 20 coauthors, 2010a, *ApJL*, 713, L87
- Jenkins, J. M., Chandrasekaran, H., McCauliff, S. D., et al., 2010b, *Proc. SPIE*, 7740, 77400
- Koch, D. G., Borucki, W. J., Basri, G., et al. 2010, *ApJL*, 713, L79
- Kron, G. E. 1952, *ApJ*, 115, 301
- Kunkel, W. E. 1975, *IAU Symp.*, 67, 15
- Kwee, K. K., van Woerden, H., 1956, *BAN*, 12, 327
- Lacy, C.H., Moffett, T.J., & Evans, D. S. 1976, *ApJS*, 30, 85
- Leto, G., Pagano, I., Buemi, C. S., & Rodonó, M. 1997, *A&A*, 327, 1114
- Lopez Arroyo, M. 1961, *The Observatory*, 81, 205
- Marcy, G. W. & Chen, G. H., 1992, *ApJ*, 390, 550
- Matijević, G., Prša, A., Orosz, J. A., et al. 2012, *AJ*, 143, 123
- Mavridis, L.N., & Avgoloupis, S. 1986, *A&A*, 154, 171
- Mirzoyan, L.V., 1990. *IAUS* 137, 1
- Motulsky, H., 2007, "GraphPad Prism 5: Statistics Guide", San Diego, CA: GraphPad Software Inc. Press, 94
- Muirhead, P.S., Becker, J., Feiden, G.A., et al., 2014, *ApJS*, 213, 5
- Muirhead, P.S.; Vanderburg, A.; Shporer, A.; et al., 2013, *ApJ*, 767, 111
- Pettersen, B.R., Coleman, L.A., & Evans, D.S. 1984, *ApJ*, 282, 214
- Pettersen, B.R., 1991, *Mem. Soc. Astron. Ital.*, 62, 217
- Pigatto, L., 1990, in *IAU Symp.* 137, "Flare Stars in Star Clusters", Associations and the Solar Vicinity (Dordrecht: Kluwer), 117
- Ribárik, G., 2002, "Occasional Technical Notes from Konkoly Observatory" No. 12, available at <http://www.konkoly.hu/staff/ribarik/SML/>
- Ribárik, G., Oláh, K. & Strassmeier, K. G., 2003, *AN*, 324, 202
- Ritter, H. & Kolb, U., 2003, *A&A*, 404, 301
- Rodonó, M., 1986, *NASSP*, 492, 409
- Scargle, J.D., 1982, *ApJ*, 263, 835
- Skumanich, A., 1972, *ApJ* 171, 565
- Slawson, R., Prša, A., Welsh, W. F., et al. 2011, *AJ*, 142, 160
- Spanier, J., & Oldham, K. B., 1987, "An Atlas of Function", Washington, DC: Hemisphere Publishing Corporation Press, 233
- Stanek, W. 1972, *Sol. Phys.*, 27, 89
- Stauffer, J. R., 1991, in *Proc. "NATO Advanced Research Workshop on Angular Momentum Evolution of Young Stars"*, ed. S. Catalano & J. R. Stauffer (Dordrecht: Kluwer), 117
- Szabó, R., Szabó, Gy. M., Dályá, G., Simon, A.E., Hodosán, G., Kiss, L.L., 2013, *A&A*, 553, 17
- Thomas, J.H., & Weiss, N.O., 2008, "Sunspots and Starspots", by John H. Thomas and Nigel O. Weiss. ISBN 978-0-521-86003-1 (HB). Published by Cambridge University Press, Cambridge, UK
- Tran, K., Levine, A., Rappaport, S., et al., 2013, *ApJ*, 774, 81
- Walker, A.R. 1981, *MNRAS*, 195, 1029

Walkowicz, L.M., Basri, G., Valenti, J.A., 2013a, ApJS, 205, 17

Walkowicz, L.M. & Basri, G.S., 2013b, MNRAS, 436, 1883

Yoldaş, E. and Dal, H.A., 2016, PASA, 33, 16

Yoldaş, E. and Dal, H.A., 2017, RmxAA, 53, 67

Zacharias, N.; Monet, D. G.; Levine, S. E.; et al., 2004, AAS, 205, 4815

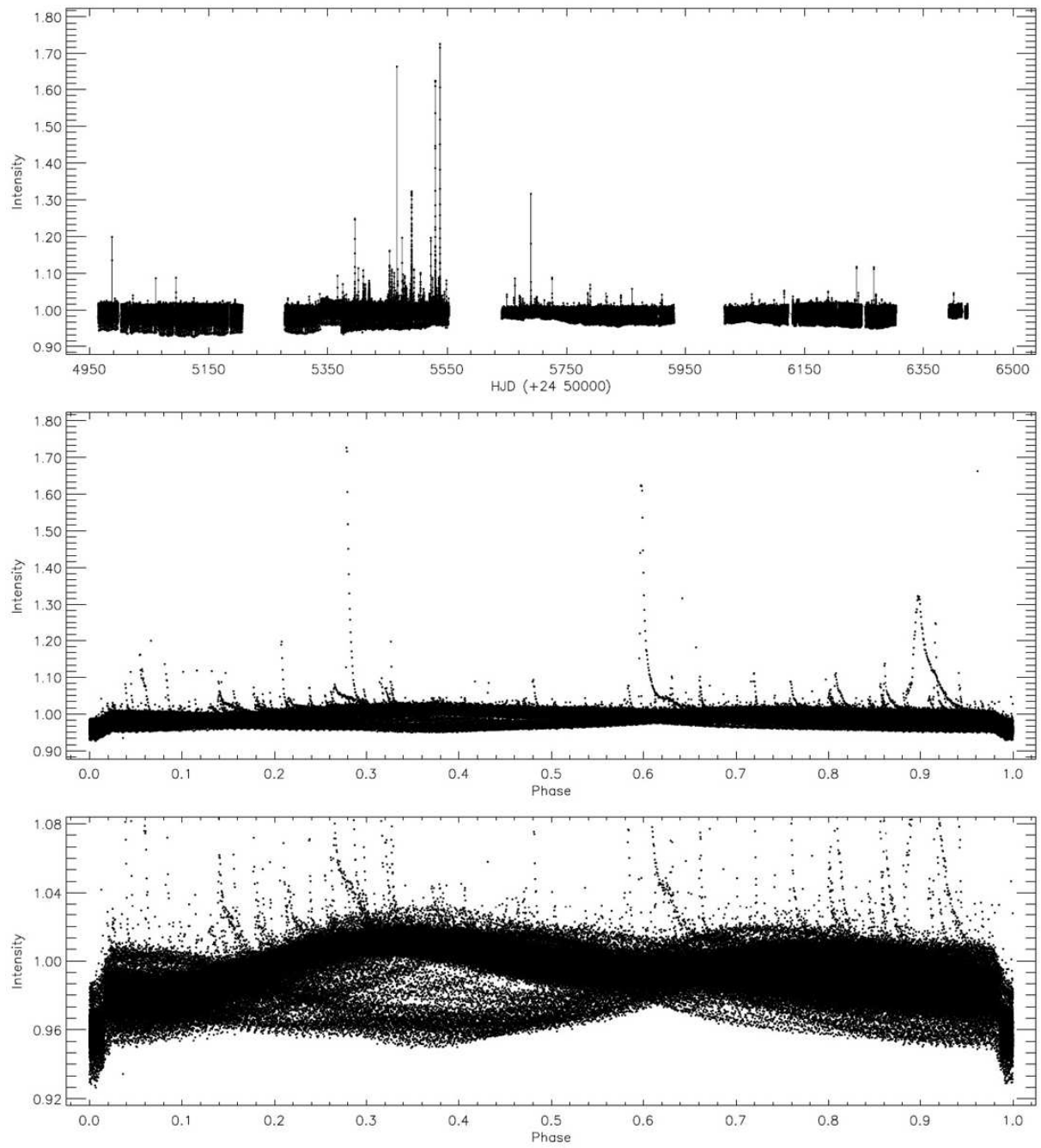


Figure 1: All of the Long Cadence and Short Cadence data taken from the Kepler Database for the KOI-256 are shown. The light variation was plotted in the plane of intensity taken from database as detrended form versus the phase computed by using orbital period.

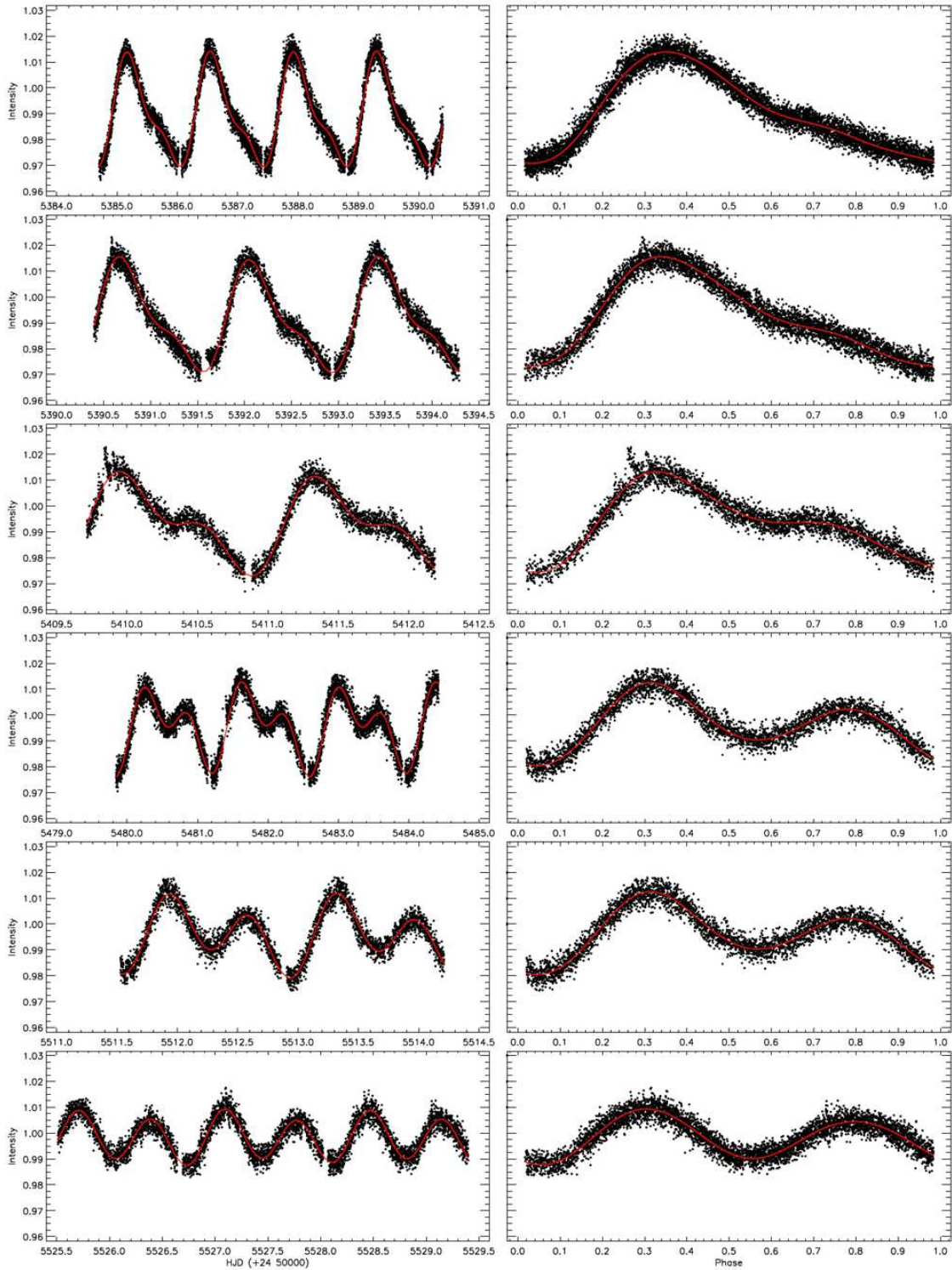


Figure 2: The observed light curve samples and their synthetic model fits derived by the SPOTMODEL analyses. In the figure, the filled circles represent the observations as intensity in detrended form, while the lines (red) represent the synthetic fits. In the left panels, the data and synthetic model are plotted versus time as Heliocentric Julian Day, while they are plotted versus phase computed using epoch and orbital period given in Equation (6) in the right panels.

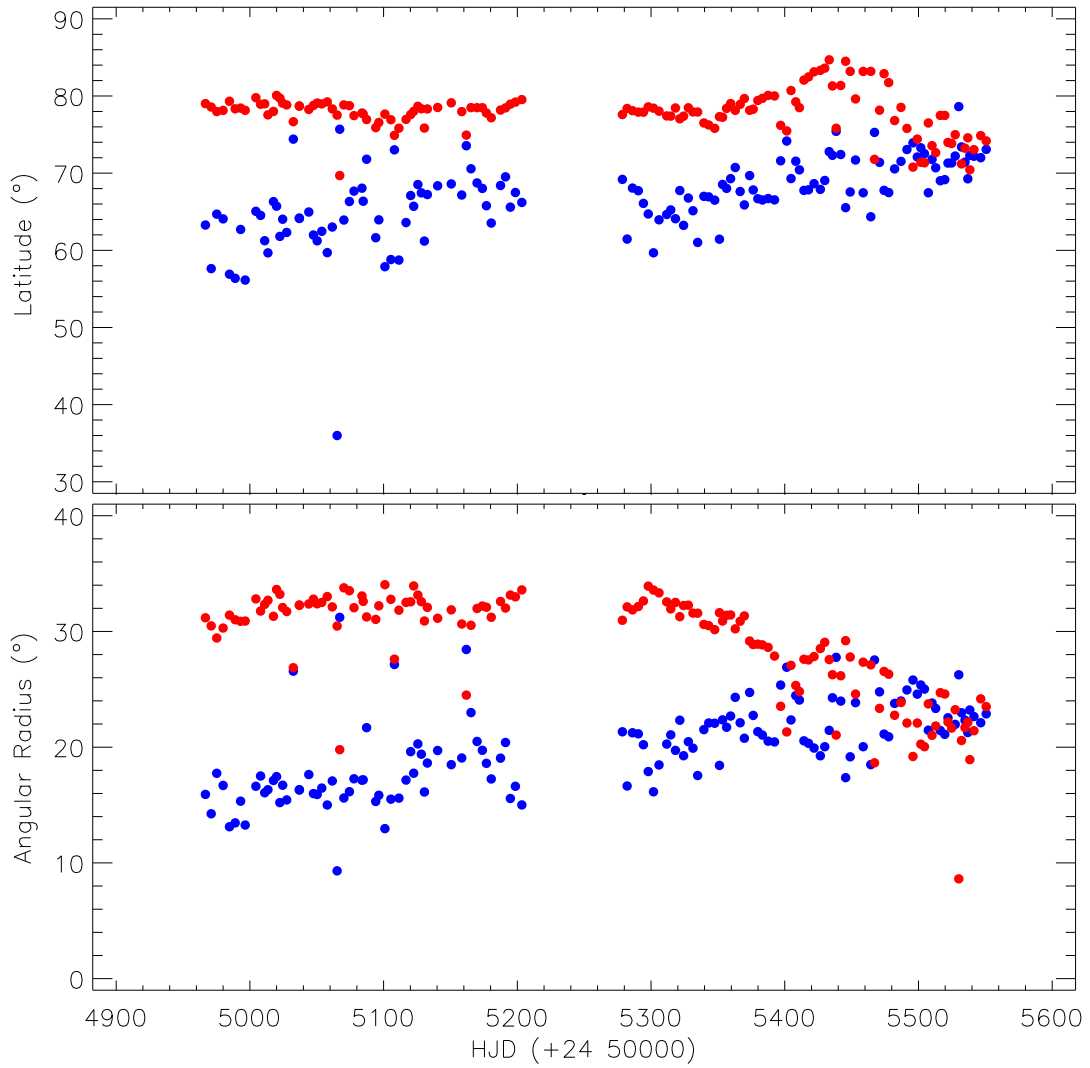


Figure 3: The variations of both spot latitude and spot radius parameters obtained with the SPOTMODEL program versus time. The filled blue circles represent the first spot and the filled red circles represent the second spot.

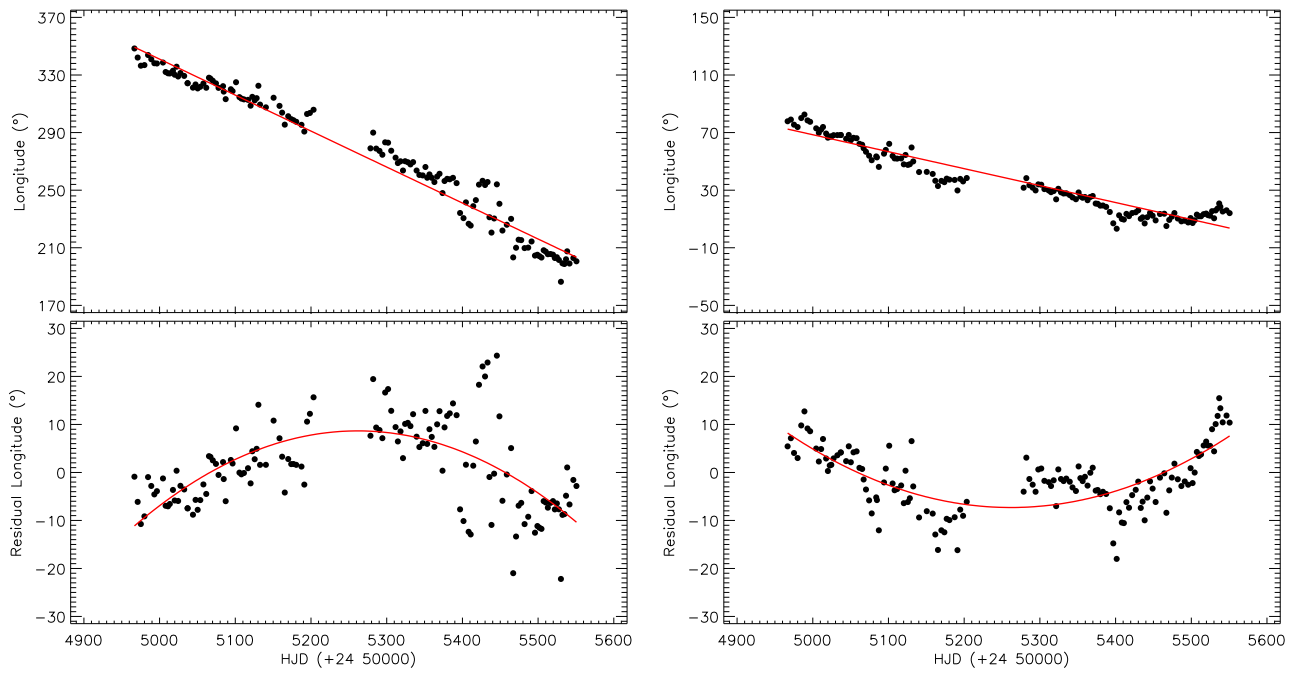


Figure 4: The variations of the first spot longitude as degree (left) and the second spot (right) are shown in the upper, while the residuals after the linear correction to the longitude variations are shown in the lower panel.

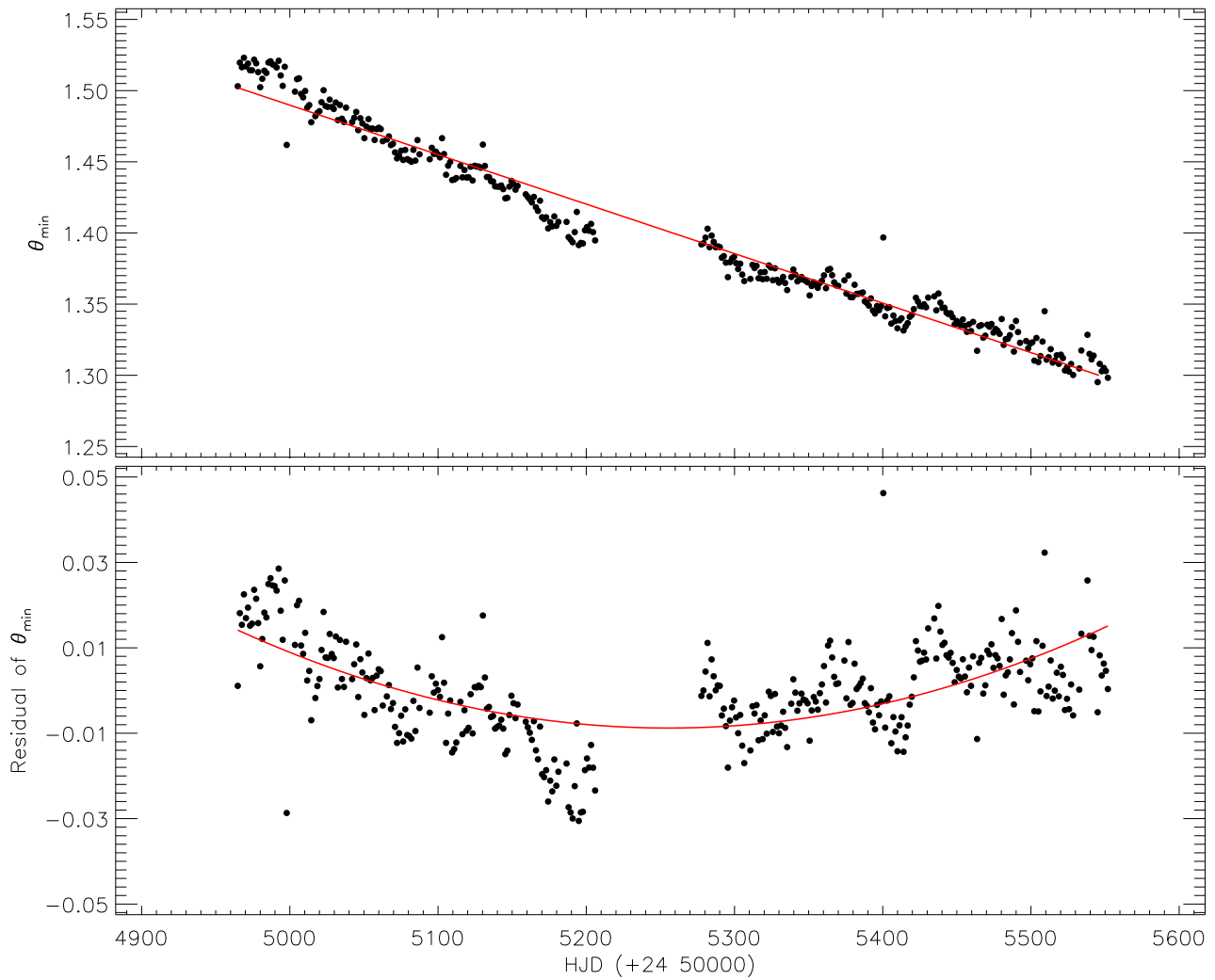


Figure 5: $O - C$ diagram for the observed minima times of sinusoidal variation versus time in each data subset shown with θ_{min} term and its linear fit are shown in the upper panel. The filled circles represent the θ_{min} variation, while the line (red) show the linear fit. In the bottom panel, the residuals of θ_{min} is shown with its parabolic fit, which is plotted to show the trends clearly for the readers.

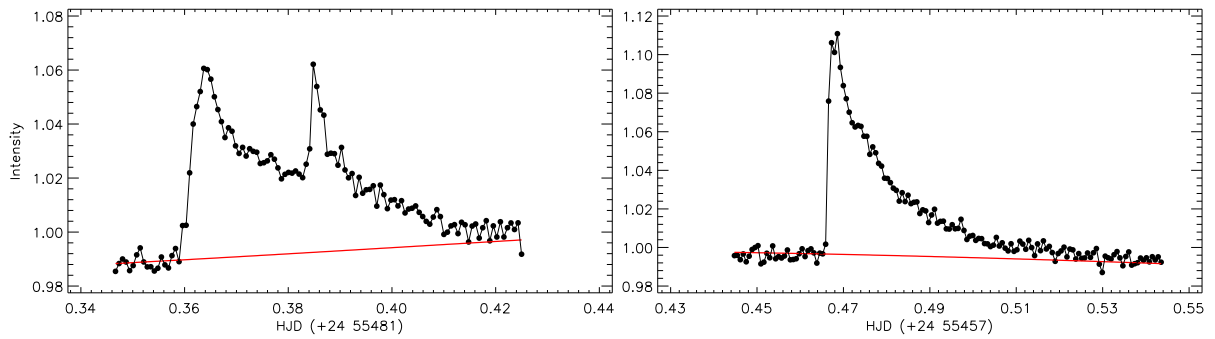


Figure 6: Two flare examples detected from the system. The light variation was plotted in the plane of intensity taken from database as detrended form versus time. The filled black circles represent the observations, while the red lines represent the quiescent level modelled by the Fourier method.

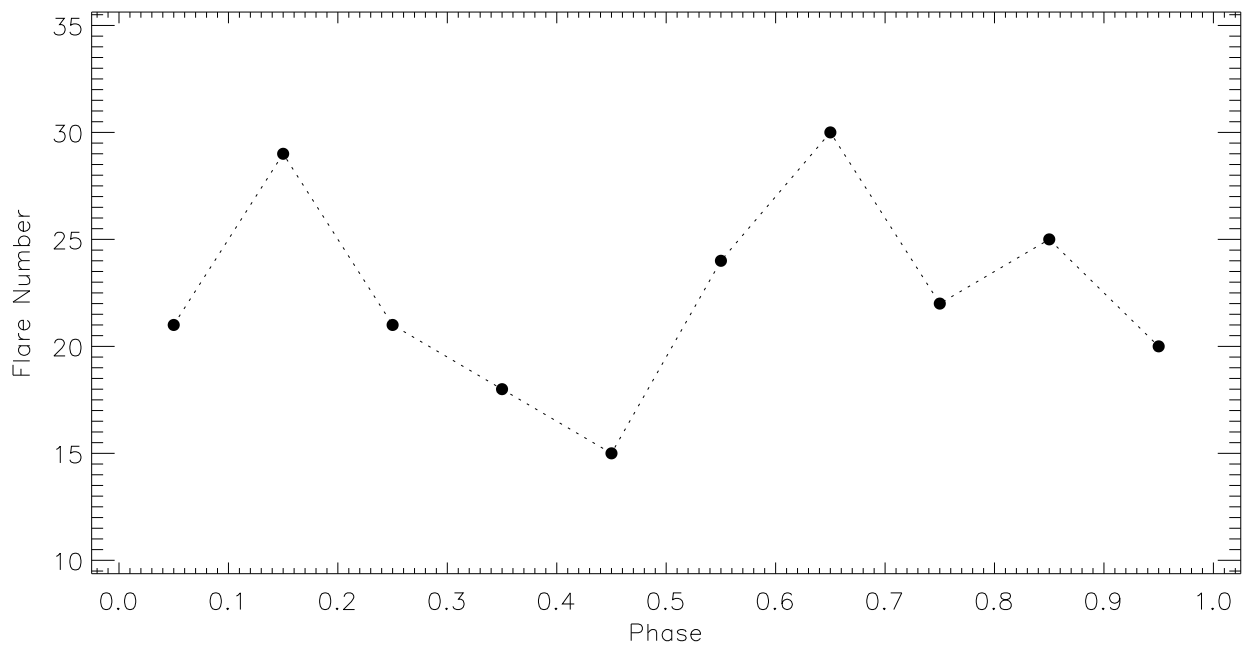


Figure 7: The distribution of flare total number in phase range of 0.10 is plotted versus the phase computed by using orbital period for 225 flares.

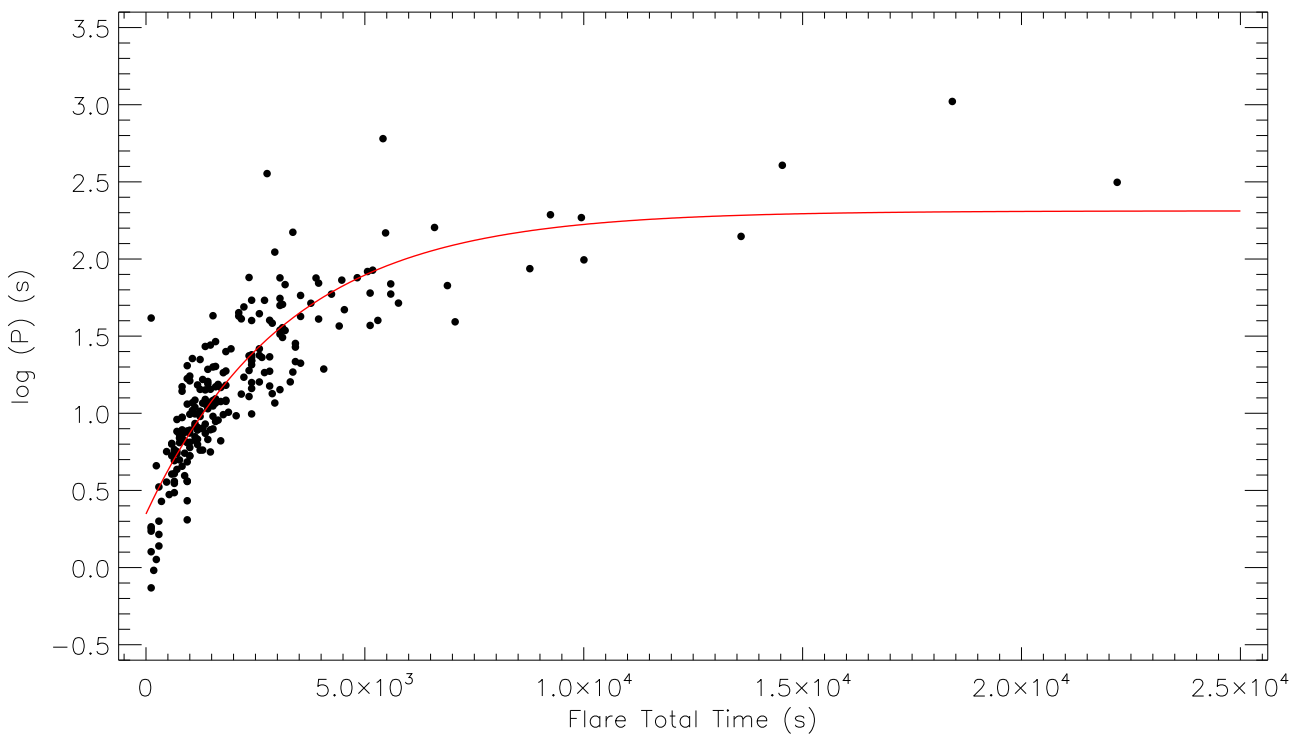


Figure 8: The distribution of the equivalent duration in the logarithmic scale ($\log P$) are plotted versus the flare total time, which were sum of flare rise and decay times. The OPEA model obtained over 225 flare determined in the analyses. The fill circles represent the observed flares, while the red line represents the OPEA model.

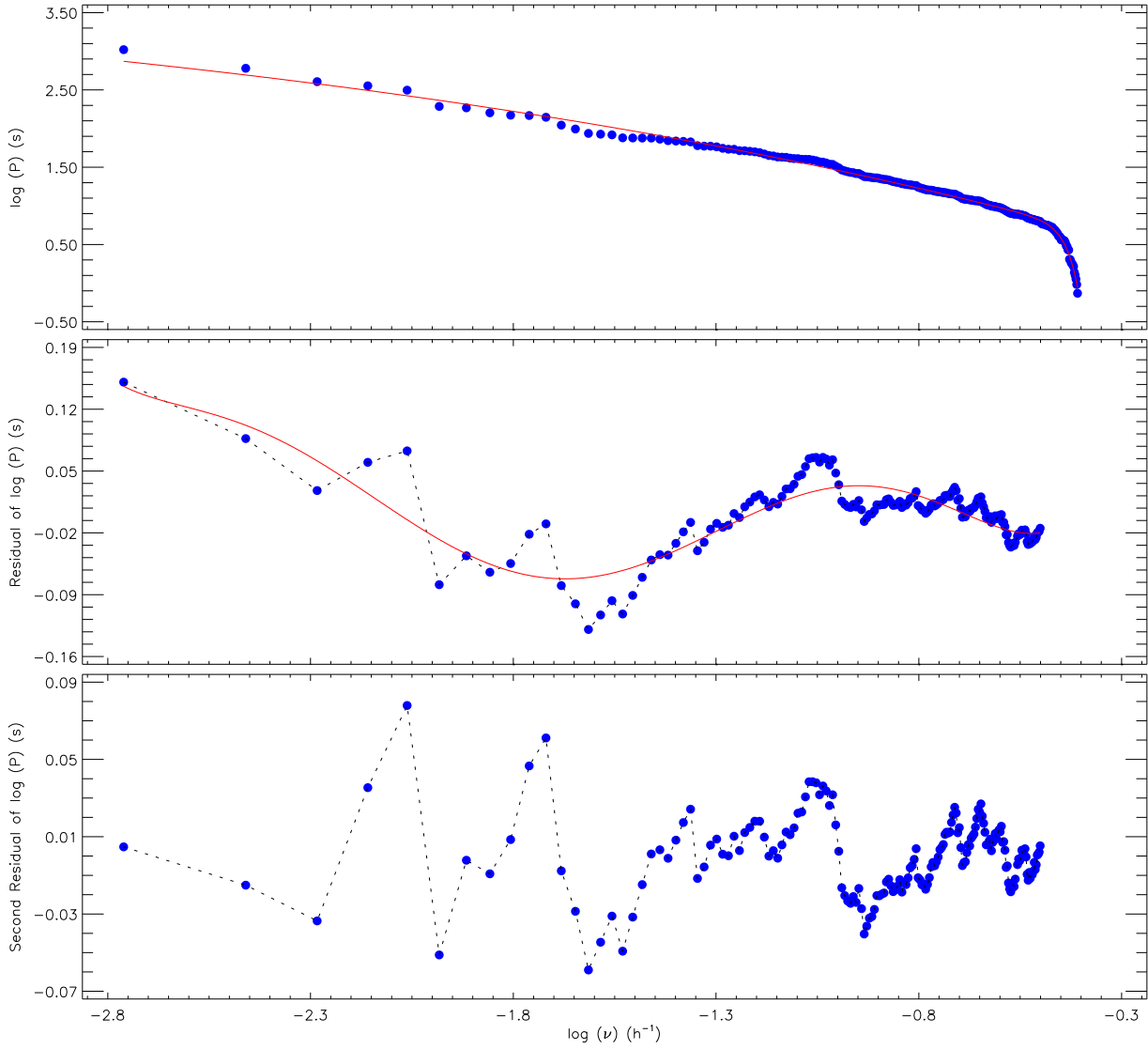


Figure 9: The cumulative flare frequencies ($\log\nu$) and model computed for 225 flares obtained from KOI-256. In the upper panel, it is seen the variation of the flare equivalent durations in logarithmic scale ($\log P$) versus the cumulative flare frequency, which is called the flare energy spectrum (Gershberg 2005), while the residuals obtained from the model are shown in the middle and bottom panels.

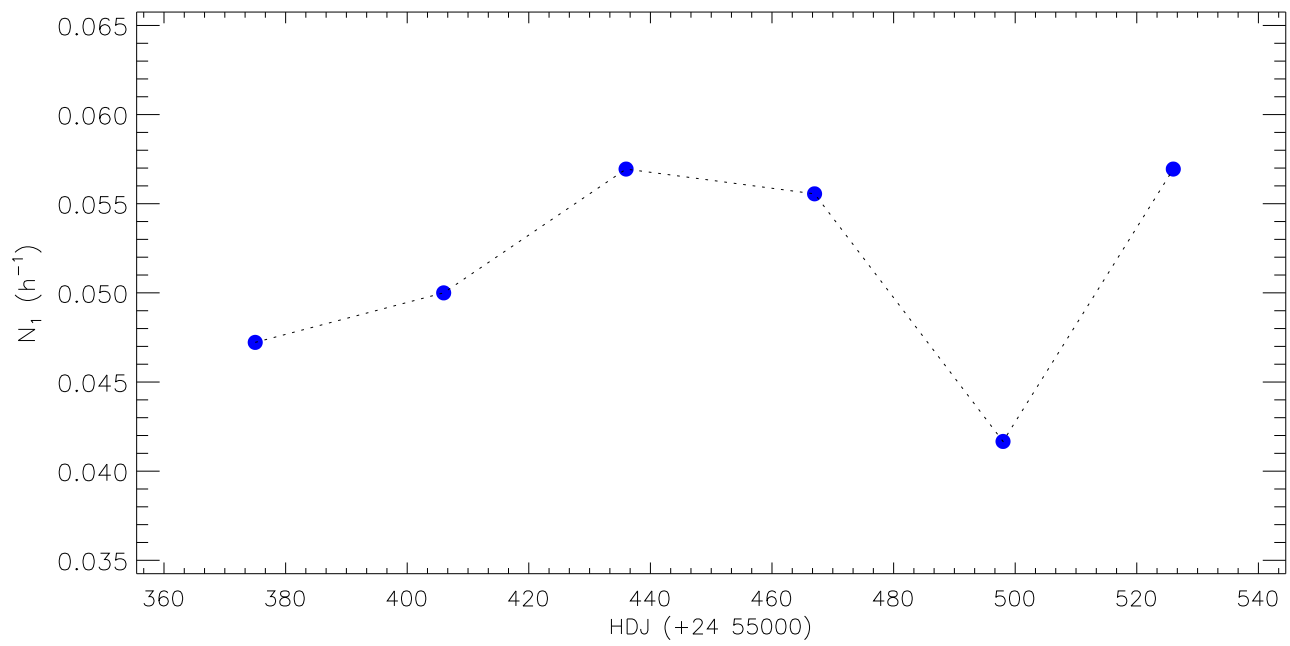


Figure 10: The monthly variation of the flare frequency of N_1 , which indicates total flare number per each hour, for KOI-256 is shown for the entire observing season.

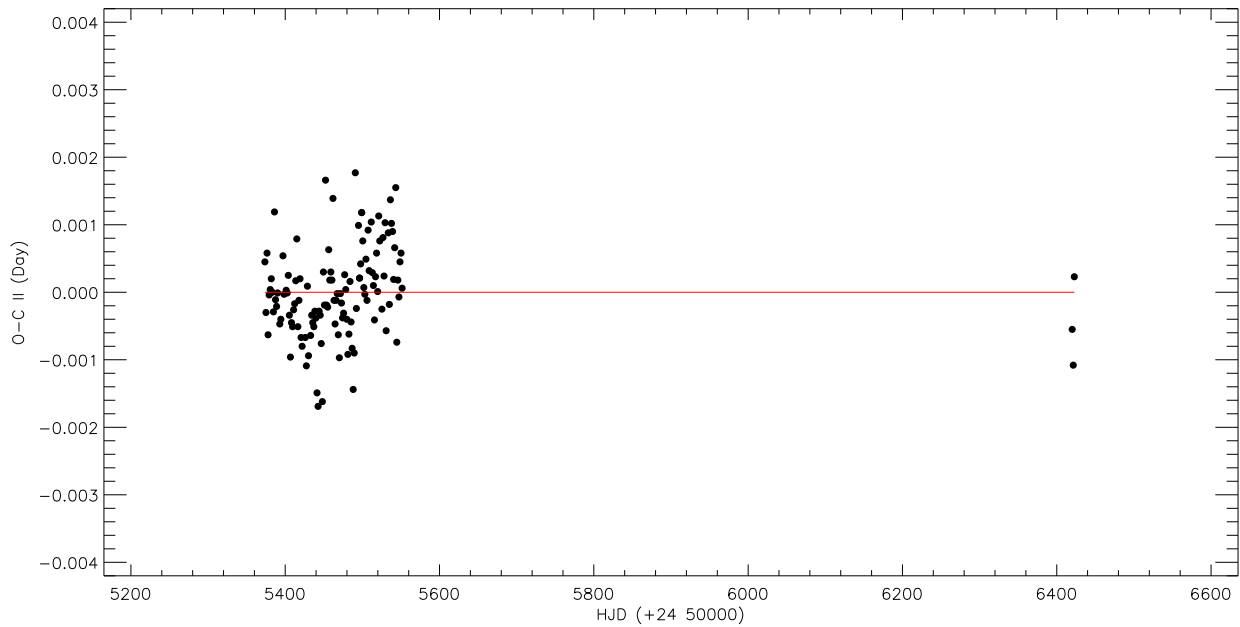


Figure 11: The variations of minima time's residuals ($O - C$)II obtained by applying a linear correction to minima times are shown versus time. All the residuals are shown with filled circles, while the red line represents a linear fit.

Table 1: Physical parameters of KOI-256 taken from the literature.

P_{orb}	(<i>day</i>)	1.3786548 ⁽¹⁾
a	(<i>AU</i>)	0.0250 ⁽¹⁾
i	($^{\circ}$)	89.3 ⁽²⁾
$(B - V)$	(<i>m</i>)	1.42 ⁽³⁾
R_1	(R_{\odot})	0.540 ⁽¹⁾
R_2	(R_{\odot})	0.01345 ⁽¹⁾
T_1	(<i>K</i>)	3450 ⁽¹⁾
T_2	(<i>K</i>)	7100 ⁽¹⁾
M_1	(M_{\odot})	0.51 ⁽¹⁾
M_2	(M_{\odot})	0.592 ⁽¹⁾
$[M/H]$	-	0.31 ⁽¹⁾
d	(<i>pc</i>)	155 ⁽⁴⁾
J, H, K	(<i>m</i>)	12.701 - 12.000 - 11.782 ⁽⁵⁾
Spectral Type	-	M3 V + WD ⁽⁴⁾

⁽¹⁾ - Muirhead et al. (2013)⁽²⁾ - Slawson et al. (2011)⁽³⁾ - Walkowicz & Basri (2013b)⁽⁴⁾ - Muirhead et al. (2014)⁽⁵⁾ - Zacharias et al. (2004)

Table 2: The Spot parameters obtained with SPOTMODEL.

JD	b_1 (Latitude)	b_2 (Latitude)	g_1 (Radius)	g_2 (Radius)	l_1 (Longitude)	l_2 (Longitude)
54966.74992763.277	$\pm 3.43079.015$	$\pm 0.25215.917$	$\pm 1.80831.179$	$\pm 0.41077.848$	$\pm 1.494378.418$	± 2.961
54971.06154157.628	$\pm 4.70478.572$	$\pm 0.23414.244$	$\pm 1.64330.481$	$\pm 0.31379.038$	$\pm 1.083342.094$	± 2.181
54975.23011164.687	$\pm 2.30377.990$	$\pm 0.32317.743$	$\pm 1.49829.433$	$\pm 0.49275.469$	$\pm 1.578336.431$	± 3.112
54979.96061464.074	$\pm 2.66978.130$	$\pm 0.25016.693$	$\pm 1.53330.294$	$\pm 0.40173.857$	$\pm 1.447336.859$	± 2.638
54984.74219956.901	$\pm 5.58879.318$	$\pm 0.19013.122$	$\pm 1.72331.410$	$\pm 0.25980.089$	$\pm 1.018343.844$	± 1.955
54988.99248956.368	$\pm 4.17378.341$	$\pm 0.17313.458$	$\pm 1.27231.008$	$\pm 0.20482.514$	$\pm 0.806340.931$	± 1.367
54993.05886762.702	$\pm 3.01478.436$	$\pm 0.21115.332$	$\pm 1.40730.875$	$\pm 0.28978.478$	$\pm 1.145338.160$	± 1.944
54996.49178456.142	$\pm 6.66678.138$	$\pm 0.25913.270$	$\pm 2.00730.898$	$\pm 0.32577.494$	$\pm 1.324337.974$	± 2.173
55004.48147165.054	$\pm 3.03079.779$	$\pm 0.21816.620$	$\pm 1.90432.811$	$\pm 0.42672.950$	$\pm 1.555338.632$	± 3.309
55007.98589264.527	$\pm 2.46478.929$	$\pm 0.23417.507$	$\pm 1.55931.759$	$\pm 0.40969.841$	$\pm 1.448332.064$	± 2.888
55011.06119561.244	$\pm 5.07678.986$	$\pm 0.34916.060$	$\pm 2.37032.337$	$\pm 0.48972.068$	$\pm 1.765331.181$	± 3.486
55013.49282759.668	$\pm 4.70477.560$	$\pm 0.75916.324$	$\pm 1.49832.693$	$\pm 0.28973.878$	$\pm 3.926331.057$	± 2.571
55017.64089966.308	$\pm 2.30377.999$	$\pm 0.75917.122$	$\pm 1.53331.309$	$\pm 0.32569.324$	$\pm 9.060332.951$	± 3.291
55019.94992165.718	$\pm 2.98880.074$	$\pm 0.23417.455$	$\pm 2.07133.626$	$\pm 0.48266.448$	$\pm 1.757330.176$	± 3.845
55022.42241161.803	$\pm 6.93879.715$	$\pm 0.31615.211$	$\pm 3.22233.209$	$\pm 0.58167.316$	$\pm 2.231335.756$	± 4.538
55024.49643864.030	$\pm 4.38179.073$	$\pm 0.38316.711$	$\pm 2.56632.067$	$\pm 0.61367.204$	$\pm 2.127328.939$	± 4.392
55027.52063362.317	$\pm 3.42278.843$	$\pm 0.20715.440$	$\pm 1.62331.722$	$\pm 0.32568.190$	$\pm 1.271331.344$	± 2.327
55032.47580674.406	$\pm 2.18576.669$	$\pm 0.20726.567$	$\pm 3.70726.866$	$\pm 3.59847.323$	$\pm 1.324301.919$	± 2.630
55036.99164664.178	$\pm 3.00778.693$	$\pm 0.27216.326$	$\pm 1.64732.266$	$\pm 0.36368.294$	$\pm 1.406324.269$	± 2.377
55036.99164664.124	$\pm 3.02078.697$	$\pm 0.27116.296$	$\pm 1.64532.273$	$\pm 0.36168.314$	$\pm 1.399324.309$	± 2.366
55044.05145464.961	$\pm 2.45878.258$	$\pm 0.28517.635$	$\pm 1.56432.375$	$\pm 0.40365.672$	$\pm 1.476321.194$	± 2.559
55047.52515761.982	$\pm 3.97078.775$	$\pm 0.29015.990$	$\pm 1.88832.788$	$\pm 0.37568.351$	$\pm 1.422323.413$	± 2.575
55050.30411561.227	$\pm 4.05979.092$	$\pm 0.29415.909$	$\pm 1.87432.386$	$\pm 0.38664.700$	$\pm 1.411320.649$	± 2.736
55053.76758962.461	$\pm 2.43078.973$	$\pm 0.21016.465$	$\pm 1.24532.507$	$\pm 0.27666.362$	$\pm 0.981321.805$	± 1.907
55057.87471059.698	$\pm 3.86979.232$	$\pm 0.19915.005$	$\pm 1.54233.013$	$\pm 0.26566.069$	$\pm 1.045324.048$	± 1.938
55061.63445663.015	$\pm 2.97478.326$	$\pm 0.26917.080$	$\pm 1.63332.120$	$\pm 0.39362.205$	$\pm 1.452321.125$	± 2.605
55065.23072735.995	$\pm 2.97477.523$	$\pm 0.798 9.311$	$\pm 1.633 30.464$	$\pm 0.82661.544$	$\pm 3.690328.098$	± 4.977
55067.18211175.691	$\pm 1.29469.690$	$\pm 5.53131.217$	$\pm 1.98219.782$	$\pm 5.43324.124$	$\pm 9.473279.457$	± 2.929
55070.27775663.922	$\pm 3.50878.844$	$\pm 0.16915.607$	$\pm 1.90933.771$	$\pm 0.35256.672$	$\pm 1.575325.965$	± 2.571
55074.42571166.321	$\pm 3.44578.750$	$\pm 0.18716.152$	$\pm 2.28333.518$	$\pm 0.45853.919$	$\pm 2.210324.187$	± 3.291
55077.84827967.671	$\pm 4.06677.458$	$\pm 0.35717.269$	$\pm 3.31132.052$	$\pm 0.86550.804$	$\pm 1.324321.033$	± 5.382
55083.82498468.052	$\pm 2.60077.793$	$\pm 0.20317.142$	$\pm 2.12233.066$	$\pm 0.50553.435$	$\pm 2.540322.217$	± 3.232
55084.73426466.361	$\pm 5.31777.680$	$\pm 0.47817.179$	$\pm 3.82732.598$	$\pm 0.95252.764$	$\pm 1.324318.453$	± 2.377
55087.27819271.806	$\pm 3.21476.954$	$\pm 0.71921.685$	$\pm 4.85931.254$	$\pm 2.17146.173$	$\pm 1.324313.208$	± 2.366
55094.10283161.631	$\pm 6.29575.903$	$\pm 0.50415.308$	$\pm 2.93231.042$	$\pm 0.66955.341$	$\pm 2.659320.091$	± 3.583
55096.42198563.947	$\pm 4.85676.563$	$\pm 0.39015.843$	$\pm 2.60432.215$	$\pm 0.55757.951$	$\pm 2.617318.779$	± 3.213
55100.97855557.876	$\pm 5.88777.649$	$\pm 0.17012.960$	$\pm 1.87234.039$	$\pm 0.23662.181$	$\pm 1.227324.958$	± 1.532

Table 2: Continued.

JD	b_1 (Latitude)	b_2 (Latitude)	g_1 (Radius)	g_2 (Radius)	l_1 (Longitude)	l_2 (Longitude)
55105.45339058.804	$\pm 5.54276.923$	$\pm 0.33815.505$	$\pm 2.26432.774$	$\pm 0.45053.787$	$\pm 1.688314.621$	± 2.377
55108.08924873.020	$\pm 2.97574.902$	$\pm 0.24127.145$	$\pm 5.19527.606$	$\pm 4.97132.067$	$\pm 1.324291.603$	± 2.366
55111.43004258.736	$\pm 3.46675.829$	$\pm 0.24115.596$	$\pm 1.41631.835$	$\pm 0.30551.917$	$\pm 1.171313.049$	± 1.653
55116.76304863.599	$\pm 2.68876.973$	$\pm 0.26417.157$	$\pm 1.59232.509$	$\pm 0.39652.047$	$\pm 1.535312.718$	± 2.365
55120.23665167.100	$\pm 2.53477.592$	$\pm 0.38219.611$	$\pm 2.22232.561$	$\pm 0.71947.943$	$\pm 2.692308.686$	± 4.336
55122.48427565.708	$\pm 2.53478.011$	$\pm 0.59417.748$	$\pm 4.26133.933$	$\pm 1.02854.446$	$\pm 4.318314.813$	± 2.782
55125.61051568.529	$\pm 2.42778.667$	$\pm 0.36020.282$	$\pm 2.67733.143$	$\pm 0.92147.553$	$\pm 3.319312.377$	± 2.022
55128.22593167.447	$\pm 3.10478.347$	$\pm 0.39319.391$	$\pm 2.93332.574$	$\pm 0.94548.032$	$\pm 3.430313.894$	± 2.197
55130.51442061.196	$\pm 6.09575.843$	$\pm 0.61516.127$	$\pm 2.98030.903$	$\pm 0.78259.660$	$\pm 2.665322.497$	± 4.008
55132.71095967.228	$\pm 2.46778.319$	$\pm 0.35118.628$	$\pm 2.02832.079$	$\pm 0.61449.971$	$\pm 2.332309.434$	± 3.950
55140.40395868.362	$\pm 1.57278.515$	$\pm 0.25319.713$	$\pm 1.62131.138$	$\pm 0.59842.595$	$\pm 2.093307.516$	± 3.901
55150.58977968.603	$\pm 2.41379.115$	$\pm 0.20318.488$	$\pm 2.40431.868$	$\pm 0.72742.700$	$\pm 2.881314.182$	± 2.219
55158.41560767.166	$\pm 3.51177.979$	$\pm 0.50019.066$	$\pm 3.17730.642$	$\pm 1.13241.285$	$\pm 3.827308.543$	± 2.145
55161.85856673.557	$\pm 1.87574.930$	$\pm 0.50028.440$	$\pm 2.85524.497$	$\pm 0.28922.522$	$\pm 2.332273.844$	± 2.366
55165.35261170.567	$\pm 3.03778.492$	$\pm 0.56222.987$	$\pm 4.48730.529$	$\pm 0.32532.892$	$\pm 2.093295.508$	± 1.653
55169.88874568.733	$\pm 3.31478.484$	$\pm 0.56220.493$	$\pm 3.74431.984$	$\pm 1.41936.448$	$\pm 1.324301.355$	± 2.571
55173.86297568.021	$\pm 4.60778.484$	$\pm 0.71519.730$	$\pm 4.60232.198$	$\pm 1.58735.569$	$\pm 1.324299.308$	± 3.291
55176.88707365.779	$\pm 3.26877.793$	$\pm 0.46318.602$	$\pm 2.49532.093$	$\pm 0.76738.022$	$\pm 2.685298.566$	± 4.758
55180.49351863.531	$\pm 4.17477.176$	$\pm 0.47617.253$	$\pm 2.45131.224$	$\pm 0.67437.329$	$\pm 2.391297.495$	± 3.965
55187.44078768.403	$\pm 3.20478.177$	$\pm 0.54419.051$	$\pm 2.97332.592$	$\pm 0.93237.112$	$\pm 1.147295.397$	± 2.693
55191.15963269.524	$\pm 3.21578.457$	$\pm 0.61020.404$	$\pm 3.62132.022$	$\pm 1.34229.811$	$\pm 1.449290.715$	± 2.285
55194.78653465.594	$\pm 4.56078.938$	$\pm 0.27315.563$	$\pm 2.67733.146$	$\pm 0.50937.822$	$\pm 2.447302.929$	± 3.696
55198.55647667.491	$\pm 3.68879.212$	$\pm 0.26816.620$	$\pm 2.75132.992$	$\pm 0.61636.101$	$\pm 2.754303.617$	± 2.496
55203.36852966.201	$\pm 3.40479.536$	$\pm 0.14915.008$	$\pm 1.96533.587$	$\pm 0.32638.443$	$\pm 1.768305.854$	± 2.577
55278.56486969.191	$\pm 2.17477.595$	$\pm 0.73621.329$	$\pm 2.21430.962$	$\pm 0.97731.706$	$\pm 3.075279.055$	± 2.056
55282.11019261.455	$\pm 3.69278.379$	$\pm 0.35816.646$	$\pm 1.80132.119$	$\pm 0.42138.373$	$\pm 1.415289.975$	± 2.653
55286.11528968.067	$\pm 2.20478.100$	$\pm 0.70221.246$	$\pm 2.11131.863$	$\pm 0.87533.457$	$\pm 2.514278.883$	± 2.760
55290.47798767.725	$\pm 2.82677.905$	$\pm 0.80921.153$	$\pm 2.58032.151$	$\pm 1.01631.765$	$\pm 3.020277.276$	± 2.495
55294.29918266.081	$\pm 2.68277.905$	$\pm 0.62920.212$	$\pm 2.09832.634$	$\pm 0.72829.837$	$\pm 2.170274.620$	± 4.009
55297.91603864.709	$\pm 3.00378.589$	$\pm 0.35017.892$	$\pm 1.87733.916$	$\pm 0.44534.050$	$\pm 1.583283.230$	± 2.813
55301.82919259.677	$\pm 3.51478.421$	$\pm 0.27116.143$	$\pm 1.51333.575$	$\pm 0.30033.796$	$\pm 1.050282.969$	± 1.885
55305.96712563.953	$\pm 2.07478.028$	$\pm 0.30318.464$	$\pm 1.28333.333$	$\pm 0.34430.741$	$\pm 1.147277.405$	± 1.998
55311.72957764.647	$\pm 2.10377.422$	$\pm 0.48820.267$	$\pm 1.50232.553$	$\pm 0.52829.781$	$\pm 1.449272.577$	± 2.740
55314.72319465.233	$\pm 1.98977.395$	$\pm 0.58821.063$	$\pm 1.52631.947$	$\pm 0.61028.626$	$\pm 1.609268.837$	± 3.056
55318.24810164.094	$\pm 2.39578.449$	$\pm 0.47119.721$	$\pm 1.56732.508$	$\pm 0.49929.410$	$\pm 1.307270.048$	± 2.801
55321.50736367.747	$\pm 2.15877.049$	$\pm 0.83022.326$	$\pm 1.98631.277$	$\pm 0.93023.642$	$\pm 2.585263.668$	± 2.343
55324.32728863.231	$\pm 1.82877.392$	$\pm 0.36119.259$	$\pm 1.11932.241$	$\pm 0.36030.961$	$\pm 1.027270.101$	± 1.825
55327.89306166.778	$\pm 2.17578.474$	$\pm 0.57020.473$	$\pm 1.75332.267$	$\pm 0.63228.538$	$\pm 1.718269.419$	± 3.508

Table 2: Continued.

JD	b_1 (Latitude)	b_2 (Latitude)	g_1 (Radius)	g_2 (Radius)	l_1 (Longitude)	l_2 (Longitude)
55331.34644565	1.131 ± 1.99577	0.933 ± 0.49119	1.913 ± 1.40931	1.583 ± 0.50427	1.701 ± 1.431	267.882 ± 2.688
55334.85091261	0.023 ± 3.03677	0.925 ± 0.41117	1.550 ± 1.48431	1.577 ± 0.39427	1.811 ± 1.149	269.490 ± 2.184
55339.48947666	0.995 ± 2.16876	0.507 ± 0.85921	1.517 ± 1.80830	0.605 ± 0.84526	0.610 ± 2.198	263.648 ± 3.641
55343.12676066	0.924 ± 1.60376	0.246 ± 0.67322	0.089 ± 1.33830	0.500 ± 0.65624	0.992 ± 1.652	260.579 ± 2.749
55347.60184266	0.501 ± 1.50675	0.809 ± 0.60522	0.068 ± 1.20730	0.153 ± 0.59323	0.722 ± 1.523	260.257 ± 2.451
55351.15738361	0.440 ± 2.74977	0.325 ± 0.49618	0.424 ± 1.45331	1.620 ± 0.44628	0.428 ± 1.200	266.097 ± 2.191
55353.48687368	0.538 ± 1.99277	0.246 ± 0.89722	0.360 ± 1.85030	0.903 ± 0.91325	0.707 ± 2.319	258.643 ± 3.919
55356.49068768	0.026 ± 2.09178	0.397 ± 0.78421	0.722 ± 1.89231	1.396 ± 0.83524	0.741 ± 2.067	260.950 ± 4.201
55359.49449869	0.289 ± 2.48479	0.019 ± 0.36122	0.689 ± 2.53831	1.424 ± 0.28925	0.281 ± 2.819	258.597 ± 2.118
55362.97850670	0.732 ± 1.76078	0.142 ± 0.57024	0.305 ± 1.95630	0.223 ± 0.32523	0.033 ± 2.644	255.656 ± 2.010
55366.63620067	0.624 ± 1.95878	0.918 ± 0.84722	0.111 ± 1.78730	0.882 ± 0.85825	0.284 ± 1.788	259.436 ± 4.395
55369.78303865	0.885 ± 2.32579	0.667 ± 0.71720	0.771 ± 1.80831	1.341 ± 0.72125	0.963 ± 1.545	261.395 ± 4.223
55373.72337969	0.688 ± 0.73478	0.148 ± 0.51924	0.727 ± 0.74129	0.172 ± 0.51720	0.718 ± 0.884	248.008 ± 1.984
55376.39375767	0.823 ± 0.83578	0.289 ± 0.44722	0.743 ± 0.77528	0.870 ± 0.45920	0.538 ± 0.897	256.363 ± 2.215
55379.84572966	0.688 ± 0.65779	0.422 ± 0.26621	0.339 ± 0.55428	0.900 ± 0.28219	0.259 ± 0.559	257.882 ± 1.646
55383.28577766	0.523 ± 0.76479	0.697 ± 0.29721	0.045 ± 0.62828	0.839 ± 0.31119	0.361 ± 0.608	257.566 ± 1.866
55387.55168566	0.708 ± 0.59580	0.077 ± 0.21320	0.520 ± 0.48628	0.623 ± 0.23118	0.404 ± 0.466	258.571 ± 1.482
55392.34307766	0.536 ± 0.71180	0.006 ± 0.26420	0.452 ± 0.56627	0.872 ± 0.28314	0.864 ± 0.561	254.923 ± 1.804
55396.93080071	0.601 ± 0.46276	0.197 ± 0.55625	0.365 ± 0.44123	0.531 ± 0.519	6.999 ± 0.799	234.162 ± 1.513
55401.46436574	0.165 ± 0.77875	0.475 ± 1.24326	0.908 ± 0.73821	0.316 ± 1.208	3.240 ± 1.728	230.587 ± 2.751
55404.65985369	0.298 ± 0.67880	0.712 ± 0.44122	0.353 ± 0.66127	0.070 ± 0.43312	0.554 ± 0.654	241.520 ± 2.359
55408.23438171	0.552 ± 0.70279	0.246 ± 0.70724	0.458 ± 0.69225	0.333 ± 0.64110	0.011 ± 0.757	226.661 ± 2.048
55410.95069170	0.428 ± 0.76578	0.487 ± 0.73924	0.069 ± 0.67524	0.809 ± 0.628	9.584 ± 0.743	225.428 ± 1.920
55414.31406067	0.766 ± 0.75882	0.063 ± 0.36320	0.547 ± 0.63527	0.598 ± 0.32713	0.545 ± 0.460	238.909 ± 2.124
55417.75575367	0.843 ± 0.95182	0.471 ± 0.41820	0.333 ± 0.81727	0.539 ± 0.41311	0.979 ± 0.619	243.091 ± 3.137
55421.88945268	0.636 ± 0.77483	0.132 ± 0.28419	0.923 ± 0.71727	0.831 ± 0.33814	0.122 ± 0.559	253.879 ± 3.132
55426.61435267	0.900 ± 0.82283	0.328 ± 0.23619	0.255 ± 0.70228	0.520 ± 0.28914	0.666 ± 0.522	256.507 ± 2.886
55429.91264969	0.051 ± 1.10883	0.615 ± 0.40020	0.039 ± 1.07729	0.060 ± 0.47015	0.990 ± 0.770	253.600 ± 4.560
55433.24020672	0.787 ± 2.09484	0.692 ± 1.00721	0.453 ± 2.94027	0.567 ± 1.69110	0.110 ± 2.408	255.676 ± 18.000
55435.67858872	0.312 ± 0.85181	0.306 ± 0.80224	0.269 ± 0.96526	0.261 ± 0.81111	0.136 ± 0.960	231.213 ± 3.429
55438.42959675	0.418 ± 0.56775	0.819 ± 1.02827	0.761 ± 0.51221	0.045 ± 0.940	6.928 ± 0.997	220.547 ± 1.531
55441.87771772	0.414 ± 0.73281	0.364 ± 0.67923	0.981 ± 0.82126	0.171 ± 0.67711	0.250 ± 0.800	230.361 ± 2.831
55445.51313865	0.529 ± 1.03384	0.504 ± 0.17817	0.364 ± 0.66329	0.201 ± 0.20214	0.208 ± 0.373	254.044 ± 2.528
55448.92276567	0.560 ± 0.84283	0.195 ± 0.30619	0.168 ± 0.66027	0.787 ± 0.28412	0.294 ± 0.436	240.545 ± 2.369
55452.90383671	0.702 ± 0.64279	0.618 ± 0.65423	0.844 ± 0.61124	0.590 ± 0.570	9.030 ± 0.615	221.961 ± 1.739
55458.65100467	0.454 ± 0.60283	0.186 ± 0.29820	0.039 ± 0.47527	0.345 ± 0.23413	0.438 ± 0.248	225.998 ± 1.374
55464.32798864	0.347 ± 1.01883	0.193 ± 0.31318	0.492 ± 0.61127	0.115 ± 0.25113	0.667 ± 0.346	230.084 ± 1.759
55467.11335975	0.280 ± 0.41871	0.792 ± 0.98627	0.533 ± 0.28518	0.648 ± 0.678	5.116 ± 0.399	203.328 ± 0.491
55470.86657371	0.397 ± 0.51678	0.158 ± 0.63424	0.780 ± 0.43623	0.353 ± 0.497	9.349 ± 0.344	210.027 ± 0.862
55474.25880067	0.772 ± 0.88482	0.891 ± 0.58721	0.131 ± 0.73226	0.546 ± 0.43811	0.610 ± 0.334	215.610 ± 1.840

Table 2: Continued.

JD	b_1 (Latitude)	b_2 (Latitude)	g_1 (Radius)	g_2 (Radius)	l_1 (Longitude)	l_2 (Longitude)					
55477.71947467.483	± 0.709	81.740	± 0.445	20.901	$\pm 0.54426.305$	± 0.323	14.101	± 0.265	215.318	± 1.092	
55482.13402570.552	± 0.486	76.821	± 0.567	23.782	$\pm 0.37022.756$	± 0.410	10.330	± 0.302	209.804	± 0.649	
55486.91738671.526	± 0.541	78.525	± 0.583	23.993	$\pm 0.45923.859$	± 0.461	8.352	± 0.355	210.133	± 0.868	
55491.37347773.059	± 0.638	75.799	± 0.844	24.945	$\pm 0.51722.085$	± 0.669	8.792	± 0.687	214.372	± 1.077	
55495.87145173.925	± 0.403	70.787	± 0.776	25.801	$\pm 0.26019.198$	± 0.499	7.578	± 0.319	204.576	± 0.374	
55499.09747372.097	± 0.543	74.413	± 0.689	24.582	$\pm 0.38822.083$	± 0.490	10.643	± 0.318	205.162	± 0.476	
55501.74285873.291	± 0.506	71.403	± 0.825	25.372	$\pm 0.33920.259$	± 0.550	7.233	± 0.426	204.146	± 0.470	
55504.46759072.524	± 0.462	71.336	± 0.772	25.018	$\pm 0.29720.040$	± 0.491	9.101	± 0.280	203.230	± 0.385	
55507.36089467.462	± 0.627	76.505	± 0.487	21.467	$\pm 0.40123.736$	± 0.317	13.054	± 0.234	208.283	± 0.462	
55510.11797871.784	± 0.618	73.560	± 0.827	23.813	$\pm 0.41821.027$	± 0.554	11.875	± 0.375	207.317	± 0.535	
55512.86927370.697	± 0.476	72.657	± 0.551	23.350	$\pm 0.30721.827$	± 0.355	11.878	± 0.250	205.546	± 0.331	
55516.32618769.021	± 0.592	77.486	± 0.453	21.440	$\pm 0.41624.709$	± 0.303	13.343	± 0.212	205.681	± 0.400	
55519.66561269.159	± 0.778	77.485	± 0.562	21.107	$\pm 0.54024.592$	± 0.380	13.768	± 0.289	205.216	± 0.448	
55522.05831271.307	± 0.671	73.982	± 0.728	22.541	$\pm 0.45022.173$	± 0.476	12.652	± 0.295	202.894	± 0.441	
55524.81471971.323	± 0.815	73.845	± 0.836	21.754	$\pm 0.52921.647$	± 0.535	12.264	± 0.379	203.441	± 0.472	
55527.45125472.219	± 0.551	74.986	± 0.485	21.968	$\pm 0.38123.235$	± 0.334	15.422	± 0.205	201.570	± 0.232	
55530.12627278.627	± 0.245	-1.110	± 98.070	26.256	± 0.134	8.622	± 0.427	10.499	± 0.479	186.390	± 0.446
55532.17263773.401	± 0.513	71.201	± 0.652	22.975	$\pm 0.32220.574$	± 0.411	15.939	± 0.219	199.223	± 0.223	
55534.78091171.429	± 0.603	73.233	± 0.630	22.334	$\pm 0.38821.695$	± 0.405	17.332	± 0.239	198.730	± 0.245	
55536.87802069.268	± 0.866	74.579	± 0.801	21.263	$\pm 0.53522.150$	± 0.498	20.782	± 0.238	202.037	± 0.371	
55538.40028172.296	± 0.638	70.433	± 1.057	23.209	$\pm 0.38118.925$	± 0.606	18.506	± 0.324	207.543	± 0.393	
55541.48260772.195	± 0.414	73.048	± 0.475	22.644	$\pm 0.27021.419$	± 0.307	15.201	± 0.162	199.068	± 0.194	
55546.55886472.005	± 0.557	74.864	± 0.465	22.111	$\pm 0.39424.176$	± 0.323	16.019	± 0.208	202.905	± 0.235	
55550.65842873.082	± 0.560	74.177	± 0.524	22.881	$\pm 0.39923.505$	± 0.373	14.069	± 0.245	200.617	± 0.240	
56421.90755774.336	± 0.319	112.006	± 0.807	26.349	$\pm 0.19918.653$	± 0.451	102.414	± 0.212	111.379	± 0.257	

Table 3: The parameters calculated for each flare detected with analysis of the Short Cadence data obtained by Kepler Mission for KOI-256 are listed.

JD (+24 00000)	P (s)	T_r (s)	T_d (s)	T_t (s)	$Amplitude$ (Intensity)
55375.342090	44.20740	235.39162	2353.99133	2589.38294	0.07436
55375.947616	16.56043	176.54371	1118.15597	1294.69968	0.02621
55376.350846	15.26603	411.94483	765.05904	1177.00387	0.04393
55376.476174	22.31022	58.84790	1176.99523	1235.84314	0.05763
55377.033340	12.30394	176.55322	1176.98573	1353.53894	0.02639
55377.296257	27.67483	588.49718	882.75485	1471.25203	0.03511
55378.175597	20.63149	176.55235	2236.29206	2412.84442	0.03071
55378.328852	1.99895	58.85654	235.39248	294.24902	0.01837
55380.097067	34.60774	235.40026	2824.77888	3060.17914	0.02929
55380.590205	7.63004	58.84790	765.05731	823.90522	0.02825
55380.741416	8.25863	294.24816	823.90522	1118.15338	0.01060
55381.267930	19.27064	235.40026	1176.99264	1412.39290	0.04652
55381.637784	7.80086	529.63978	647.34336	1176.98314	0.01822
55383.117879	1.83830	58.83926	58.84704	117.68630	0.03887
55383.318131	1.72242	58.84790	58.85654	117.70445	0.02840
55385.586972	6.76596	1176.99005	235.39939	1412.38944	0.00939
55385.605363	15.97846	1176.99005	2118.58157	3295.57162	0.01176
55386.161845	1.38046	176.54285	117.70445	294.24730	0.01294
55386.294665	9.55332	176.56099	1353.53290	1530.09389	0.02204
55386.812322	10.15885	1059.29424	823.90349	1883.19773	0.01717
55389.135650	15.95644	1412.38771	1176.98832	2589.37603	0.01390
55390.912711	8.01176	470.79878	823.90176	1294.70054	0.02250
55391.021692	4.32847	353.08570	353.09520	706.18090	0.01673
55391.457613	9.42058	117.70358	706.19731	823.90090	0.02878
55392.580110	4.03619	117.70358	470.79792	588.50150	0.01606
55392.744261	9.80095	294.24643	1471.23302	1765.47946	0.01100
55393.700563	23.57782	235.39853	2118.56429	2353.96282	0.03602
55394.247507	4.93193	117.70358	529.64496	647.34854	0.02670
55395.160216	13.90038	117.70358	706.19558	823.89917	0.04806
55395.578427	404.82960	1118.12832	13417.62970	14535.75802	0.27309
55397.006747	38.35936	765.04262	2118.56947	2883.61210	0.03148
55401.269904	42.89049	117.69408	1412.37994	1530.07402	0.13944
55404.761341	7.68292	176.54198	765.04003	941.58202	0.03032
55405.599122	3.58347	117.70272	353.09174	470.79446	0.01701
55406.776100	7.62807	176.54976	529.63373	706.18349	0.03081
55407.746018	9.85367	176.54198	823.88534	1000.42733	0.02354
55408.136300	58.03656	470.79360	3060.13853	3530.93213	0.05706

Table 3: Continued.

JD (+24 00000)	P (s)	T_r (s)	T_d (s)	T_t (s)	$Amplitude$ (Intensity)
55409.594580	75.45501	235.38902	2824.75555	3060.14458	0.13119
55409.832291	34.40761	176.54976	3001.29667	3177.84643	0.04241
55409.890187	26.17318	117.70272	1824.31181	1942.01453	0.05453
55412.681417	50.01182	294.23434	2765.89642	3060.13075	0.05973
55412.876899	6.91584	176.54976	588.47904	765.02880	0.02533
55413.391825	6.37731	58.84704	529.63978	588.48682	0.02509
55414.867810	5.48103	117.70186	588.49546	706.19731	0.02086
55414.925024	12.11842	235.39680	1294.67549	1530.07229	0.01774
55416.699338	12.14917	176.54112	1647.76464	1824.30576	0.02079
55417.073953	4.53704	176.54112	647.33299	823.87411	0.01461
55417.940336	2.68543	58.84704	294.24298	353.09002	0.01618
55418.479781	7.96692	294.24298	1000.42214	1294.66512	0.01591
55418.700463	40.81725	1353.52080	2589.33802	3942.85882	0.03181
55418.793776	4.98763	176.54026	588.48595	765.02621	0.01339
55419.427897	82.95145	823.87238	4237.09920	5060.97158	0.04302
55419.497371	185.47791	1118.12400	8827.28755	9945.41155	0.07175
55421.411309	8.11929	235.38730	941.58288	1176.97018	0.02561
55423.293915	68.96291	353.08915	5237.51011	5590.59926	0.05211
55425.451690	5.81840	58.85568	588.48336	647.33904	0.02426
55425.581783	11.64399	941.58029	647.33040	1588.91069	0.02157
55427.109523	10.32274	235.38643	1000.42646	1235.81290	0.02436
55428.162527	6.31033	117.69322	470.78150	588.47472	0.02500
55429.939553	14.85190	294.24125	1294.66598	1588.90723	0.03114
55431.149892	6.49379	117.70186	882.71424	1000.41610	0.02000
55431.203700	14.69386	411.95088	1294.65648	1706.60736	0.02178
55433.127822	1.64001	176.53939	117.70099	294.24038	0.01724
55433.193209	5.77048	58.84704	1176.96240	1235.80944	0.01492
55434.151534	1.12874	176.55667	58.83754	235.39421	0.01448
55434.157664	2.97310	117.69235	411.94224	529.63459	0.01664
55434.353825	6.63105	117.68371	1588.90378	1706.58749	0.01544
55435.784160	4.06328	117.70099	529.63459	647.33558	0.02182
55435.835924	0.73911	58.84618	58.85482	117.70099	0.01707
55435.926512	3.61430	235.40198	706.17312	941.57510	0.01044
55436.045026	7.41432	58.84618	1294.65389	1353.50006	0.01989
55436.068183	3.51315	117.68371	529.64237	647.32608	0.01205
55436.081125	2.71089	353.08656	588.48077	941.56733	0.00666
55436.558584	23.75906	353.08656	2236.22035	2589.30691	0.01960
55436.636912	7.82704	353.08570	823.87411	1176.95981	0.00867
55436.794249	11.70227	176.54717	882.71165	1059.25882	0.03533
55438.701360	21.11367	117.69235	3413.18621	3530.87856	0.03614

Table 3: Continued.

JD (+24 00000)	P (s)	T_r (s)	T_d (s)	T_t (s)	$Amplitude$ (Intensity)
55438.913866	5.61630	353.08570	1118.11363	1471.19933	0.01361
55441.226917	32.58644	647.32522	2412.76147	3060.08669	0.04902
55441.943445	3.33076	235.38470	58.85482	294.23952	0.02369
55443.211671	6.27441	235.39335	941.57251	1176.96586	0.01589
55443.229380	2.03953	470.78582	470.77805	941.56387	0.00682
55443.527706	0.95940	58.84618	117.70099	176.54717	0.01647
55443.531792	11.15569	235.39248	1294.64957	1530.04205	0.02500
55445.415740	11.63756	235.39248	1059.26400	1294.65648	0.02883
55446.473501	11.65998	941.56214	2000.82614	2942.38829	0.01389
55446.954364	23.94391	529.63200	1883.12429	2412.75629	0.03194
55447.452254	37.09812	1176.94598	3942.80266	5119.74864	0.01531
55450.550613	26.19646	235.39248	2353.90579	2589.29827	0.04492
55450.614637	15.81569	1118.10672	1294.65389	2412.76061	0.02139
55451.372709	5.64617	117.70099	353.08397	470.78496	0.03361
55453.086373	20.35148	176.55494	765.01325	941.56819	0.07455
55453.672806	149.01479	235.38384	3118.92422	3354.30806	0.18088
55456.080515	72.95417	529.63805	3942.77933	4472.41738	0.07085
55456.193579	12.16574	176.54544	941.55869	1118.10413	0.03073
55456.308004	15.39212	117.69149	1530.02477	1647.71626	0.02762
55456.611096	5.30449	117.69149	470.77546	588.46694	0.02077
55456.622675	12.84198	235.38298	2118.51763	2353.90061	0.01174
55457.468608	193.53680	411.92842	8827.13117	9239.05958	0.11971
55458.638065	6.67818	235.38298	882.72029	1118.10326	0.01673
55460.915679	9.38679	58.84531	765.02016	823.86547	0.02893
55460.929301	3.05990	117.70013	529.62854	647.32867	0.00933
55461.137038	10.42624	58.84531	1000.41091	1059.25622	0.03052
55461.401988	84.63194	176.54630	5002.01914	5178.56544	0.10579
55462.177765	11.80962	353.08224	1118.11104	1471.19328	0.02530
55463.505896	16.78388	117.70013	823.85597	941.55610	0.05735
55464.891260	15.02389	1471.18291	1353.49142	2824.67434	0.01315
55465.276084	10.70152	117.68198	1294.65475	1412.33674	0.02691
55465.425926	14.17575	176.54544	1176.93734	1353.48278	0.04345
55465.482458	18.31911	235.39939	1530.01958	1765.41898	0.05152
55465.952419	41.43259	58.84618	58.84531	117.69149	0.68383
55467.303046	68.23197	117.70013	3060.06336	3177.76349	0.13012
55469.090940	10.93777	176.53680	941.55350	1118.09030	0.03609
55469.613346	18.50133	823.85424	2530.43395	3354.28819	0.01302
55470.019964	6.44893	117.70013	823.85338	941.55350	0.02676
55470.607755	4.84475	117.69926	823.85424	941.55350	0.01444
55471.355605	15.53370	235.39075	1176.93475	1412.32550	0.03245

Table 3: Continued.

JD (+24 00000)	P (s)	T_r (s)	T_d (s)	T_t (s)	$Amplitude$ (Intensity)
55472.217880	19.35750	176.54458	3883.92019	4060.46477	0.01227
55472.319364	5.77485	411.93533	882.69869	1294.63402	0.01891
55472.813844	16.21783	117.70013	882.70733	1000.40746	0.05861
55473.593024	51.78851	235.39075	5531.62435	5767.01510	0.03109
55474.398085	12.41232	294.22742	1294.64179	1588.86922	0.02210
55474.727057	44.88099	176.52730	1941.95923	2118.48653	0.18575
55474.900057	9.91234	176.54458	941.55264	1118.09722	0.03113
55475.423824	5.64696	117.69926	588.47126	706.17053	0.02536
55475.562087	6.45265	58.83667	706.17053	765.00720	0.03652
55476.091984	29.14921	235.38989	1353.48710	1588.87699	0.08591
55476.294952	7.44200	58.84531	941.56042	1000.40573	0.02985
55476.567392	314.03759	706.16189	21479.19898	22185.36086	0.07990
55476.696120	21.90776	529.61731	1883.11219	2412.72950	0.02629
55476.823486	86.57508	117.69926	8650.51920	8768.21846	0.03453
55478.800721	21.97714	765.00634	1647.72144	2412.72778	0.02521
55479.075204	48.89291	235.39853	2000.80195	2236.20048	0.08979
55479.596246	75.63241	411.92582	4413.52886	4825.45469	0.06286
55480.878077	3.63981	235.38125	706.16966	941.55091	0.00691
55480.897829	53.97274	176.54458	2530.42618	2706.97075	0.07388
55480.934608	46.92281	294.23520	4236.99120	4531.22640	0.02365
55481.363701	147.57825	470.77978	5001.99754	5472.77731	0.07048
55481.384815	160.06194	2295.02765	4295.83565	6590.86330	0.07118
55482.448012	25.10970	235.38989	1588.86576	1824.25565	0.07721
55484.817558	7.04579	117.69062	1000.40400	1118.09462	0.03365
55486.206319	8.58246	176.52730	941.55869	1118.08598	0.02701
55486.736215	5.60687	58.84531	588.47818	647.32349	0.01998
55487.396200	39.15742	1941.95318	5119.68989	7061.64307	0.01433
55488.308191	75.29180	353.07965	3530.81722	3883.89686	0.07725
55488.373577	9.90490	529.62422	1883.10701	2412.73123	0.01054
55489.807290	140.09412	3942.74909	9650.89814	13593.64723	0.02690
55490.681140	1049.43937	2471.56790	15947.53056	18419.09846	0.33241
55493.194394	14.87307	176.53594	647.32262	823.85856	0.04763
55494.570213	54.05090	353.07965	2059.64986	2412.72950	0.11057
55494.645815	28.36075	941.54832	2471.57482	3413.12314	0.01765
55498.618661	9.03055	176.54371	1471.17168	1647.71539	0.01734
55498.702436	3.62009	176.54371	470.77891	647.32262	0.01493
55498.718101	13.40445	588.46867	2295.02074	2883.48941	0.01675
55499.032768	5.29147	176.54458	823.84906	1000.39363	0.00952
55500.394283	15.19193	117.68198	1706.55984	1824.24182	0.03291
55501.954679	6.79482	58.85395	1118.09117	1176.94512	0.02542

Table 3: Continued.

JD (+24 00000)	P (s)	T_r (s)	T_d (s)	T_t (s)	$Amplitude$ (Intensity)
55502.011891	18.73455	588.46781	2236.18406	2824.65187	0.01551
55502.410333	11.46807	176.53507	765.01238	941.54746	0.03713
55504.495855	9.53926	117.69840	1118.08339	1235.78179	0.02625
55505.411932	55.53928	176.54371	2883.49718	3060.04090	0.08309
55505.476636	60.13398	117.69840	5001.98198	5119.68038	0.10543
55508.166292	1.79399	58.84531	58.85395	117.69926	0.03583
55508.891661	14.28894	235.38902	1000.40141	1235.79043	0.04915
55509.218588	21.62582	706.16794	2706.95347	3413.12141	0.01718
55509.391587	31.00352	294.24298	2824.65274	3118.89571	0.03682
55510.390758	36.78295	176.55235	4236.96960	4413.52195	0.05801
55510.739480	11.95360	882.70214	941.54832	1824.25046	0.02207
55511.376307	51.67114	588.46867	3177.72288	3766.19155	0.05542
55513.722008	9.63831	176.53507	1883.10442	2059.63949	0.01544
55514.407193	8.84904	117.69062	1471.17946	1588.87008	0.02198
55515.838861	13.31654	235.38902	1941.94195	2177.33098	0.01942
55516.291791	11.92080	353.07965	1353.48106	1706.56070	0.02661
55516.392594	39.99328	3118.89658	2177.32234	5296.21891	0.01812
55516.430735	23.22504	117.68976	2706.95434	2824.64410	0.02021
55517.760920	98.70816	3177.73325	6826.23677	10003.97002	0.02622
55520.294607	67.24819	176.54371	6708.53923	6885.08294	0.03740
55522.737707	39.92723	176.53594	2236.18666	2412.72259	0.03204
55522.816034	75.88575	176.53507	2177.34134	2353.87642	0.19217
55524.700634	23.03246	58.84531	2353.87728	2412.72259	0.03093
55525.479130	50.79022	353.08051	2765.81174	3118.89226	0.09610
55526.711920	9.11512	117.69926	588.47818	706.17744	0.03393
55527.096741	8.51295	117.69840	1235.77661	1353.47501	0.01772
55527.229556	7.92308	353.07965	1176.93907	1530.01872	0.01985
55527.828923	17.13460	176.53507	2059.64467	2236.17974	0.03384
55528.409901	6.92449	176.54458	647.31485	823.85942	0.01744
55530.246145	602.45858	353.08051	5060.84976	5413.93027	0.62493
55530.609853	110.84606	529.62509	2412.72605	2942.35114	0.13490
55530.638459	22.64046	58.84531	1000.40400	1059.24931	0.05504
55531.639676	20.11803	823.86029	765.01498	1588.87526	0.03575
55532.322138	5.99543	58.84531	941.55091	1000.39622	0.02514
55532.377988	17.43303	117.69926	882.69696	1000.39622	0.04528
55532.540771	19.95533	117.69926	1412.32205	1530.02131	0.05189
55534.100491	11.44830	117.69926	1235.78698	1353.48624	0.01969
55534.874221	7.51594	117.70013	765.00634	882.70646	0.03108
55535.983734	69.75887	235.38125	3707.37907	3942.76032	0.07953
55536.041628	40.06649	117.69926	2706.97334	2824.67261	0.04786

Table 3: Continued.

JD (+24 00000)	P (s)	T_r (s)	T_d (s)	T_t (s)	$Amplitude$ (Intensity)
55536.117911	27.10988	117.69149	1235.78698	1353.47846	0.07168
55536.827618	59.17967	882.70646	3354.28214	4236.98861	0.03548
55538.078801	357.68647	176.54458	2589.26717	2765.81174	0.71509
55538.144186	40.92859	117.69926	2059.64986	2177.34912	0.07322
55539.366763	7.80770	117.69062	706.17139	823.86202	0.02386
55540.609774	23.02603	235.38125	2412.73296	2648.11421	0.04814
55540.952368	5.51462	117.68285	765.02534	882.70819	0.01524
55540.963266	18.93492	117.69062	2236.19702	2353.88765	0.02537
55541.343321	3.94267	117.70013	765.00806	882.70819	0.01674
55541.395084	14.23128	411.93533	2648.12371	3060.05904	0.01220
55542.043493	1.26695	58.85395	58.84618	117.70013	0.02280
55542.082316	7.81970	176.53594	1294.64438	1471.18032	0.02129
55542.610851	26.84851	529.62682	2883.52397	3413.15078	0.03662
55542.691222	7.77636	117.69926	882.70819	1000.40746	0.02239
55542.725277	4.57177	58.84531	176.53680	235.38211	0.04254
55543.163907	14.31275	411.92669	1059.25363	1471.18032	0.03769
55544.722950	7.26750	176.52816	588.48077	765.00893	0.03342
55545.570242	5.29618	176.54544	823.86374	1000.40918	0.01745
55545.611108	16.07877	235.39075	1176.94598	1412.33674	0.05000
55547.527733	35.88220	588.46435	2530.43914	3118.90349	0.02779
55548.411805	6.62462	176.53680	706.17398	882.71078	0.01821
55548.777558	42.66308	117.69149	2000.81146	2118.50294	0.09381
55549.246839	14.48484	117.70013	2295.04061	2412.74074	0.01299
55550.629480	18.35971	470.78237	2236.19616	2706.97853	0.01681
55552.452797	10.20249	353.08310	882.72029	1235.80339	0.03406
56419.872987	42.42996	235.39507	3295.63123	3531.02630	0.07203
56421.178735	18.79582	176.54630	1647.81994	1824.36624	0.02747
56422.598915	59.26194	2707.13491	2883.67258	5590.80749	0.02899

Table 4: Parameters derived from the OPEA model by least squares method.

Parameter	Values	95% Confidence Intervals
y_0	0.34741	0.2440 to 0.4508
<i>Plateau</i>	2.3121	2.1232 to 2.5010
K	0.00031033	0.00024245 to 0.00037821
τ	3222.4	2644.0 to 4124.6
<i>Half - time</i>	2233.6	1832.7 to 2859.0
<i>Span</i>	1.9647	1.7914 to 2.1380
R^2	-	0.75

Table 5: Minima times and their residuals.

MJD (Obs)	E	Type	$O - C(I)$ (day)	$O - C(II)$ (day)	linear fit to the $O - C(I)$
55373.637352	296	I	0.00175	0.00045	0.00130
55375.015258	297	I	0.00100	-0.00030	0.00130
55376.394783	298	I	0.00188	0.00058	0.00130
55377.772232	299	I	0.00068	-0.00063	0.00130
55379.151475	300	I	0.00127	-0.00004	0.00130
55380.530204	301	I	0.00135	0.00004	0.00131
55381.909019	302	I	0.00151	0.00020	0.00131
55383.287462	303	I	0.00130	0.00000	0.00131
55384.665830	304	I	0.00102	-0.00029	0.00131
55386.045957	305	I	0.00250	0.00119	0.00131
55387.423309	306	I	0.00120	-0.00011	0.00131
55388.801861	307	I	0.00110	-0.00021	0.00132
55390.180721	308	I	0.00131	-0.00001	0.00132
55392.937562	310	I	0.00085	-0.00047	0.00132
55394.316284	311	I	0.00092	-0.00040	0.00132
55397.074523	313	I	0.00186	0.00054	0.00133
55398.452606	314	I	0.00130	-0.00003	0.00133
55401.209976	316	I	0.00136	0.00003	0.00133
55402.588586	317	I	0.00133	-0.00001	0.00133
55403.967495	318	I	0.00158	0.00025	0.00133
55405.345561	319	I	0.00100	-0.00034	0.00134
55406.723591	320	I	0.00038	-0.00096	0.00134
55408.102754	321	I	0.00089	-0.00045	0.00134
55409.481348	322	I	0.00084	-0.00051	0.00134
55410.860243	323	I	0.00108	-0.00026	0.00134
55412.238990	324	I	0.00118	-0.00017	0.00135
55413.617981	325	I	0.00152	0.00017	0.00135
55414.997250	326	I	0.00214	0.00079	0.00135
55416.374600	327	I	0.00084	-0.00051	0.00135
55417.753642	328	I	0.00123	-0.00012	0.00135
55419.132621	329	I	0.00156	0.00020	0.00135
55420.510400	330	I	0.00069	-0.00067	0.00136
55421.888921	331	I	0.00056	-0.00080	0.00136
55426.025010	334	I	0.00069	-0.00067	0.00136
55427.403240	335	I	0.00027	-0.00109	0.00136
55428.783068	336	I	0.00145	0.00009	0.00137
55430.160693	337	I	0.00043	-0.00094	0.00137
55432.918294	339	I	0.00073	-0.00064	0.00137

Table 5: Continued.

MJD (Obs)	E	Type	$O - C(I)$ (day)	$O - C(II)$ (day)	linear fit to the $O - C(I)$
55434.297248	340	I	0.00103	-0.00034	0.00137
55435.675787	341	I	0.00092	-0.00045	0.00137
55437.054380	342	I	0.00086	-0.00051	0.00138
55438.433266	343	I	0.00110	-0.00028	0.00138
55439.811817	344	I	0.00100	-0.00038	0.00138
55441.189359	345	I	-0.00011	-0.00149	0.00138
55442.567810	346	I	-0.00031	-0.00169	0.00138
55443.947869	347	I	0.00110	-0.00028	0.00139
55445.326462	348	I	0.00104	-0.00034	0.00139
55446.704701	349	I	0.00063	-0.00076	0.00139
55448.082487	350	I	-0.00023	-0.00162	0.00139
55449.463059	351	I	0.00169	0.00030	0.00139
55450.841227	352	I	0.00121	-0.00019	0.00139
55452.221730	353	I	0.00306	0.00166	0.00140
55453.598523	354	I	0.00120	-0.00019	0.00140
55454.977153	355	I	0.00118	-0.00022	0.00140
55456.356654	356	I	0.00203	0.00063	0.00140
55457.734853	357	I	0.00158	0.00018	0.00140
55459.113623	358	I	0.00170	0.00030	0.00140
55460.492162	359	I	0.00159	0.00018	0.00141
55461.872023	360	I	0.00280	0.00139	0.00141
55463.249164	361	I	0.00129	-0.00012	0.00141
55464.627459	362	I	0.00094	-0.00047	0.00141
55466.006470	363	I	0.00130	-0.00012	0.00141
55467.385217	364	I	0.00139	-0.00002	0.00141
55468.763258	365	I	0.00078	-0.00063	0.00142
55470.141569	366	I	0.00045	-0.00097	0.00142
55471.521176	367	I	0.00140	-0.00002	0.00142
55472.899686	368	I	0.00126	-0.00016	0.00142
55474.278113	369	I	0.00104	-0.00038	0.00142
55475.656836	370	I	0.00111	-0.00031	0.00142
55477.036061	371	I	0.00169	0.00026	0.00143
55478.414494	372	I	0.00147	0.00004	0.00143
55479.792703	373	I	0.00103	-0.00040	0.00143
55481.170834	374	I	0.00051	-0.00092	0.00143
55482.549788	375	I	0.00081	-0.00062	0.00143
55483.929219	376	I	0.00159	0.00016	0.00144
55485.307269	377	I	0.00099	-0.00044	0.00144
55486.685532	378	I	0.00061	-0.00083	0.00144
55488.063580	379	I	0.00000	-0.00144	0.00144

Table 5: Continued.

MJD (Obs)	E	Type	$O - C(I)$ (day)	$O - C(II)$ (day)	linear fit to the $O - C(I)$
55489.442769	380	I	0.00054	-0.00090	0.00144
55490.824094	381	I	0.00322	0.00177	0.00144
55492.200729	382	I	0.00120	-0.00024	0.00145
55494.959266	384	I	0.00244	0.00099	0.00145
55496.337138	385	I	0.00166	0.00021	0.00145
55496.337138	385	I	0.00166	0.00021	0.00145
55497.716000	386	I	0.00187	0.00042	0.00145
55499.095410	387	I	0.00263	0.00118	0.00145
55499.095410	387	I	0.00263	0.00118	0.00145
55500.473644	388	I	0.00222	0.00076	0.00146
55501.851611	389	I	0.00153	0.00007	0.00146
55503.230158	390	I	0.00143	-0.00003	0.00146
55504.609336	391	I	0.00196	0.00049	0.00146
55505.987369	392	I	0.00134	-0.00012	0.00146
55507.367066	393	I	0.00239	0.00092	0.00146
55508.745117	394	I	0.00179	0.00032	0.00147
55511.503144	396	I	0.00251	0.00104	0.00147
55512.881040	397	I	0.00176	0.00029	0.00147
55514.259500	398	I	0.00157	0.00010	0.00147
55515.637647	399	I	0.00107	-0.00041	0.00148
55517.016941	400	I	0.00171	0.00023	0.00148
55518.395944	401	I	0.00206	0.00058	0.00148
55519.774024	402	I	0.00149	0.00001	0.00148
55521.153793	403	I	0.00261	0.00113	0.00148
55522.532080	404	I	0.00225	0.00076	0.00148
55525.288367	406	I	0.00123	-0.00025	0.00149
55526.668079	407	I	0.00230	0.00081	0.00149
55528.046162	408	I	0.00173	0.00024	0.00149
55529.425603	409	I	0.00252	0.00103	0.00149
55530.802659	410	I	0.00092	-0.00057	0.00149
55533.561410	412	I	0.00238	0.00088	0.00150
55534.939002	413	I	0.00132	-0.00018	0.00150
55536.319211	414	I	0.00288	0.00137	0.00150
55537.697510	415	I	0.00252	0.00102	0.00150
55539.076038	416	I	0.00240	0.00090	0.00150
55540.453980	417	I	0.00169	0.00019	0.00151
55541.833100	418	I	0.00216	0.00066	0.00151
55543.212646	419	I	0.00306	0.00155	0.00151
55544.589008	420	I	0.00077	-0.00074	0.00151
55545.968579	421	I	0.00169	0.00018	0.00151

Table 5: Continued.

MJD (Obs)	E	Type	$O - C(I)$ (day)	$O - C(II)$ (day)	linear fit to the $O - C(I)$
55547.346980	422	I	0.00144	-0.00007	0.00151
55548.726156	423	I	0.00197	0.00045	0.00152
55550.104937	424	I	0.00210	0.00058	0.00152
55551.483063	425	I	0.00158	0.00006	0.00152
56420.033207	1055	I	0.00206	-0.00055	0.00261
56421.411327	1056	I	0.00153	-0.00108	0.00261
56422.791294	1057	I	0.00285	0.00023	0.00261